CHAPTER TWO

Interaction Between Light and Photosynthetic Microorganisms

Laurent Pilon[1], **Razmig Kandilian**
University of California, Los Angeles, Los Angeles, CA, United States
[1]Corresponding author: e-mail address: pilon@seas.ucla.edu

Contents

Abstract

This chapter aims to introduce the physical concepts and to provide the experimental and theoretical frameworks necessary to understand and to quantify the interaction between light and photosynthetic microorganisms. Indeed, light transfer is arguably the most critical aspect to consider in designing, optimizing, and operating photobioreactors of all sizes for the production of a wide range of value-added products. This chapter presents state-of-the art theoretical and experimental methods for determining

Advances in Chemical Engineering, Volume 48
ISSN 0065-2377
http://dx.doi.org/10.1016/bs.ache.2015.12.002

the scattering phase function and the absorption and scattering cross-sections of unicellular and multicellular microorganisms as well as of colonies. An extensive database of these so-called radiation characteristics over the photosynthetically active radiation region is presented for a wide variety of promising freshwater and marine microalgae, cyanobacteria, and nonsulfur purple bacteria with various shapes, sizes, pigments, and responses to stresses. The effects of photoacclimation and of progressive and sudden nitrogen starvation on the radiation characteristics are illustrated with *Nannochloropsis oculata*. Finally, limitations of current approaches are discussed and future research directions are suggested.

1. INTRODUCTION

Photosynthetic microorganisms use sunlight as their energy source and carbon dioxide as their carbon source. Some of them are capable of producing various value-added products including (i) nutritional supplements (Richmond, 2004), (ii) biofuels such as hydrogen (Das and Veziroğlu, 2001) or lipids, in particular triglycerides (TAGs), for biodiesel production (Chisti, 2007), as well as (iii) fertilizers (Richmond, 2004; Benemann, 1979). Other species are able to remove organic waste from effluent water (Richmond, 2004).

Due to the interest in the above-mentioned applications, the cultivation of photosynthetic microorganisms in photobioreactors (PBRs) exposed to artificial light (indoor) or to sunlight (outdoor) has been studied extensively. The economic viability of large-scale cultivation can be severely reduced by poor light penetration in dense microorganism cultures (Cornet et al., 1992; Pilon et al., 2011; Béchet et al., 2013; Pruvost et al., 2014). In fact, unlike nutrient concentrations, pH, and temperature, light intensity cannot be easily homogenized in the PBRs. As discussed in detail in other chapters of this book, it is essential to accurately predict light transfer in the culture in order to design, operate, monitor, and control PBRs with optimum light availability and maximum productivity and energy conversion efficiency (Pilon et al., 2011; Cornet and Dussap, 2009). To do so, understanding and quantifying the interactions between light and photosynthetic microorganisms are essential.

This chapter aims to provide the physical concepts needed to understand and to quantify the interaction between light and photosynthetic microorganisms from both experimental and theoretical points of view. It focuses on the optical phenomena taking place up to the moment when photons are

absorbed. The subsequent biological processes and pathways involved in photosynthesis have been described in detail elsewhere (Ke, 2001; Blankenship, 2008) and need not be repeated. This chapter also discusses how the interaction between light and photosynthetic microorganisms are affected by stresses. Finally, it closes by offering a few prospects.

2. BACKGROUND

2.1 Photosynthetic Microorganisms: Shapes and Sizes

There are thousands of photosynthetic microorganism species classified as diatoms, green or red microalgae, eustigmatophytes, prymnesiophytes, and cyanobacteria (Canter-Lund and Lund, 1995; Rodolfi et al., 2009). While most diatoms and green microalgae exist in unicellular forms, cyanobacteria can be either unicellular or multicellular (Becker, 1994; Schirrmeister et al., 2013). This leads to photosynthetic microorganisms with a large variety of shapes and sizes. Fig. 1A shows a micrograph of unicellular green microalgae *Chlamydomonas reinhardtii* appearing spheroidal

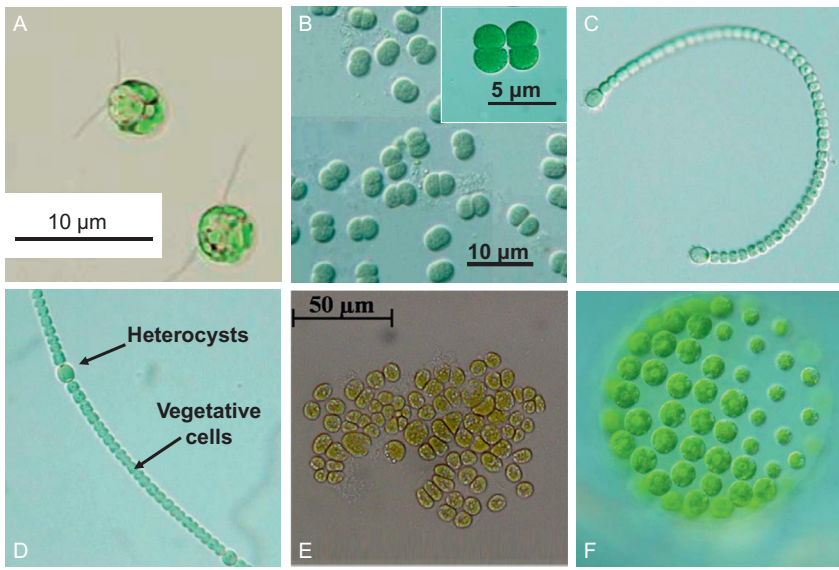

Figure 1 Micrographs of (A) *Chlamydomonas reinhardtii*, (B) dumbell-shaped *Synechocystis* sp. cell free floating and immediately after cell division (inset), (C) *Anabaenopsis* sp., (D) *Anabaena cylindrica*, (E) a colony of the microalgae *B. braunii*, and (F) *Pleodorina californica*. *Panels (B–D) and (F) are reproduced with permission from Prof. Yuuji Tsukii, Hosei University (http://protist.i.hosei.ac.jp/).*

with major and minor diameters around 7–10 μm. They have been considered for photobiological hydrogen (Benemann, 2000; Melis, 2002; Pilon and Berberoğlu, 2014) and lipids (Hu et al., 2008) production, and are often used as model systems. Fig. 1B shows a micrograph of a population of free-floating unicellular cyanobacterium *Synechocystis* sp. with a dumbbell shape whose lobs are about 3–5 μm in radius. They are also considered for biofuel production (Nakajima and Ueda, 1997). The inset of Fig. 1B shows a micrograph of *Synechocystis* sp. immediately after cell division into two morphologically identical daughter cells (Pinho et al., 2013). On the other hand, certain multicellular cyanobacteria such as *Anabaenopsis* sp., *elenkinii*, and *circularis* develop specialized cells called heterocysts that contain nitrogenase enzymes used for the biocatalytic reduction of atmospheric nitrogen into ammonia (Berman-Frank et al., 2003). This special ability to fix atmospheric nitrogen makes these cyanobacteria potential producers of fertilizers (Benemann, 1979). In addition, they are capable of producing hydrogen under certain conditions (Das and Veziroğlu, 2001; Tiwari and Pandey, 2012). Fig. 1C shows a micrograph of the cyanobacterium *Anabaenopsis* sp. consisting of spheroidal vegetative cells with 3–3.5 μm minor diameter and 4 μm major diameter and nearly spherical heterocysts 4–5 μm in diameter. Fig. 1D shows the filamentous heterocystous cyanobacterium *Anabaena cylindrica* consisting of connected and nearly spherical vegetative cells and fewer and larger heterocysts 2–4 μm in diameter. Filaments length varies widely but typically exceeds 100 μm.

Finally, several microalgae species of interest for various value-added products form colonies during their growth. For example, *Botryococcus braunii* secretes exopolysaccharides (EPS), a viscous substance coating the cell surface and causing their aggregation into colonies. EPS production is part of a protection mechanism activated in response to environmental conditions such as limited illumination (Dayananda et al., 2007), nonoptimal temperature (Demura et al., 2014), high salinity (Demura et al., 2014), and limited nutrient availability (Bayona and Garcés, 2014). In addition, a recent study demonstrated reversible cell aggregation in concentrated *Chlorella vulgaris* cultures (Souliés et al., 2013). Fig. 1E shows the colony formation of microalgae *Botryococcus braunii* consisting of tightly packed cells embedded in a semitransparent EPS matrix. These colonies resemble fractal aggregates formed by diffusion-limited aggregation (DLA). Finally, Fig. 1F illustrates how certain colonial green microalgae can form complex spherical aggregates containing a fixed number of distant cells including (i) eudorina (16, 32, or 64 cells), (ii) pleodorina (32–128 cells), or (iii) volvox (up to

50,000 cells). Note that large colonies are much easier to harvest that small free-floating cells which could prove practical and cost effective for industrial production (Lee et al., 2009).

2.2 Light Harvesting Antenna or Pigments

Photosynthetic microorganisms absorb photons in the photosynthetically active radiation (PAR) region ranging from 400 to 700 nm thanks to photosynthetic pigments, also referred to as light harvesting antenna. Each pigment absorbs light over different spectral bands of the solar spectrum enabling more efficient utilization of solar energy. Chlorophyll (Chl) *a*, *b*, and *c* molecules are the primary pigments responsible for absorbing visible photons and transferring the charges to the reaction center. Additionally, there exists a wide variety of accessory pigment carotenoids that can be divided into carotenes and xanthophylls (Ke, 2001). Carotenes are photosynthetic and absorb photons with wavelength corresponding to green and yellow colors and transfer the charges to chlorophyll molecules (Ke, 2001). They increase the solar light utilization efficiency of the microorganisms by broadening their absorption spectrum. On the other hand, xanthophylls act to protect the photosynthetic apparatus against excessive light (Ke, 2001). These photoprotective carotenoids shield the photosynthetic apparatus from photooxidation under large light intensities and convert excess radiant energy into heat (Lubián et al., 2000; Gentile and Blanch, 2001; Dubinsky and Stambler, 2009). In addition, phycobiliproteins are found in cyanobacteria and red algae (Madigan and Martinko, 2006). They include phycoerythrobilin (PEB) and phycourobilin (PUB), absorbing mainly around 500–550 nm, and phycocyanin (PCCN), absorbing strongly at 620 nm (Madigan and Martinko, 2006). Finally, bacteriochlorophylls absorb light mainly in the far to near infrared part of the electromagnetic spectrum (700–1000 nm) and are often found in purple bacteria (Ke, 2001).

Fig. 2 shows the specific absorption coefficient *Ea* (in m^2/mg) of Chl *a*, *b*, and *c*, photosynthetic (PSC) and photoprotective (PPC) carotenoids, as well as phycoerythrobilin (PEB) and phycourobilin (PUB) over the PAR region (Bidigare et al., 1990). It illustrates the two absorption peaks of Chl *a* and *b*, one in the blue and one in the red part of the visible spectrum (Ke, 2001). Chl *a* absorbs around 435, 630, and 676 nm while Chl *b* absorbs around 475 and 650 nm.

All photosynthetic species express Chl *a* but feature specific combination of other pigments. For example, marine eustigmatophycease *Nannochloropsis*

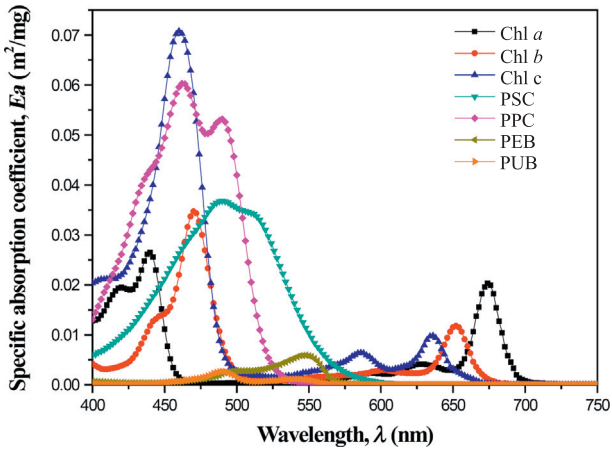

Figure 2 Specific absorption coefficient *Ea* of Chl *a*, *b*, *c*, photosynthetic (PSC) and photoprotective (PPC) carotenoids, as well as phycoerythrobilin (PEB) and phycourobilin (PUB) (Bidigare et al., 1990).

oculata contain the pigments Chl *a*, β-carotene, and the xanthophylls violaxanthin and vaucherxanthin but lack Chl *b* (Cohen, 1999). Note that advances in genetic engineering has enable the reduction of light harvesting antenna, i.e., the concentration of pigments (Nakajima and Ueda, 1997, 2000; Polle et al., 2003). For example, *Synechocystis* sp. has been genetically engineered with reduced light harvesting pigments (particularly PCCN), to increase their energetic yield per cell (Nakajima and Ueda, 1997). Similarly, *C. reinhardtii* has been genetically modified with truncated light antenna, i.e., with reduced Chl *a* and *b* pigment concentrations (Polle et al., 2003; Berberoğlu et al., 2008).

Finally, photosynthetic microorganisms not only absorb light but also scatter it due to the refractive index mismatch between the different cell compartments and between the cell wall and the surrounding growth medium (Jonasz and Fournier, 2007). Here, scattering refers to the elastic interaction between a photon and the microorganism resulting in the photon changing its direction while conserving its energy, i.e., its wavelength. Scattering depends mainly on the cell size and on the refractive index mismatch between the cell and the surrounding medium. The effective refractive index of the cell depends on their water content and their chemical composition (Jonasz and Fournier, 2007; Aas, 1996). The major cell constituents, namely, proteins, carbohydrates, and lipids do not absorb in the PAR region and have refractive indices larger than that of water. In addition,

carbohydrates and proteins have larger refractive indices than lipids. All these constituents have refractive index nearly constant over the PAR region (Aas, 1996).

2.3 Light Transfer in Photobioreactors

Fig. 3 illustrates schematically the transport of photons in a PBR and their interaction with photosynthetic microorganisms including absorption and scattering. One can distinguish between *single scattering*, when photons are subjected to at most one scattering event, and *multiple scattering* when photons may be scattered more than once. In PBRs, microorganisms are typically uniformly distributed and randomly oriented thanks to stirring and/or bubble sparging, used as ways to keep them in suspension (Kumar et al., 2011). Thus, the PBR culture can be assumed to be homogeneous, absorbing, scattering, and nonemitting. Then, the spectral radiation intensity $I_\lambda(\mathbf{r},\hat{\mathbf{s}})$ (in $W/m^2 \cdot sr \cdot nm$) along the direction $\hat{\mathbf{s}}$, at wavelength λ, and location $\mathbf{r}$ in the suspensions satisfies the radiative transfer equation (RTE) expressed as (Pilon et al., 2011)

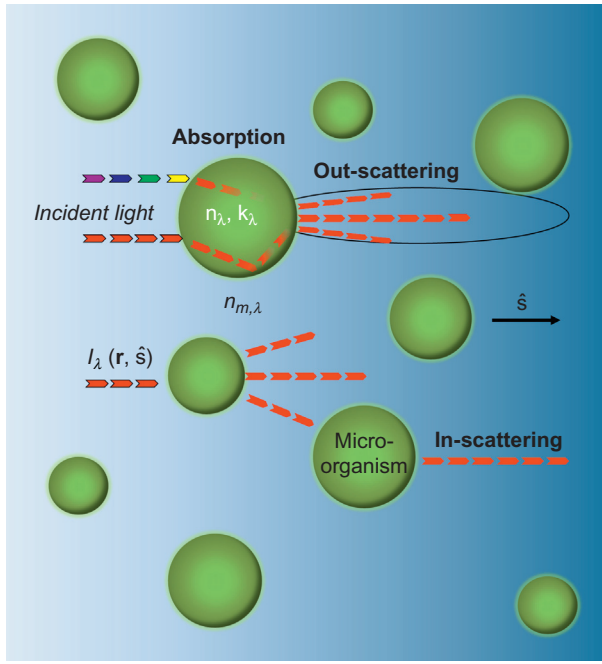

Figure 3 Illustration of light transfer in PBR including absorption and scattering of photons by photosynthetic microorganisms.

$$\hat{\mathbf{s}} \cdot \nabla I_\lambda(\mathbf{r}, \hat{\mathbf{s}}) = -\kappa_\lambda I_\lambda(\mathbf{r}, \hat{\mathbf{s}}) - \sigma_{s,\lambda} I_\lambda(\mathbf{r}, \hat{\mathbf{s}}) + \frac{\sigma_{s,\lambda}}{4\pi} \int_{4\pi} I_\lambda(\mathbf{r}, \hat{\mathbf{s}}_i) \Phi_{T,\lambda}(\hat{\mathbf{s}}_i, \hat{\mathbf{s}}) d\Omega_i. \quad (1)$$

Here, κ_λ and $\sigma_{s,\lambda}$ are the effective spectral absorption and scattering coefficients of the suspension (in m^{-1}), respectively. The extinction coefficient is defined as $\beta_\lambda = \kappa_\lambda + \sigma_{s,\lambda}$. The scattering phase function $\Phi_{T,\lambda}(\hat{\mathbf{s}}_i, \hat{\mathbf{s}})$ represents the probability that light propagating in the solid angle $d\Omega_i$ along direction $\hat{\mathbf{s}}_i$ be scattered into the solid angle $d\Omega$ along direction $\hat{\mathbf{s}}$. It is normalized such that

$$\frac{1}{4\pi} \int_{4\pi} \Phi_{T,\lambda}(\hat{\mathbf{s}}_i, \hat{\mathbf{s}}) d\Omega_i = 1. \quad (2)$$

The first and second terms on the right-hand side of Eq. (1) represent respectively the attenuation by absorption and out-scattering while the last term corresponds to the augmentation of radiation due to in-scattering (Fig. 3). This last term accounts for multiple scattering and vanishes when single scattering prevails, thus simplifying significantly the solution of the RTE.

Moreover, it is often interesting to define integral variables describing the scattering phase function $\Phi_{T,\lambda}$ in simpler terms. For example, the asymmetry factor, denoted by g_λ, for an axisymmetric phase function is defined as (Pilon et al., 2011)

$$g_\lambda = \frac{1}{2} \int_0^\pi \Phi_{T,\lambda}(\Theta) \cos\Theta \sin\Theta \, d\Theta \quad (3)$$

where Θ is the scattering angle between directions $\hat{\mathbf{s}}_i$ and $\hat{\mathbf{s}}$. The asymmetry factor varies between -1 and 1, corresponding to the limiting cases of purely backward and forward scattering, respectively. On the other hand, isotropic scattering features $\Phi_{T,\lambda}(\Theta) = 1$ and $g_\lambda = 0$. Similarly, the backward scattering ratio, denoted by b_λ, is defined as (Pottier et al., 2005)

$$b_\lambda = \frac{1}{2} \int_{\pi/2}^\pi \Phi_{T,\lambda}(\Theta) \sin\Theta d\Theta. \quad (4)$$

It is equal to 0, 1/2, and 1 for purely forward, isotropically, and purely backward scattering suspensions, respectively. Note that photosynthetic microorganism suspensions scatter visible light strongly in the forward direction due to their large dimensions compared with the wavelength. Then, g_λ approaches unity and b_λ tends to zero.

The average absorption $\bar{C}_{abs,\lambda}$ and scattering $\bar{C}_{sca,\lambda}$ cross-sections (in m^2) of a suspension of polydisperse microorganism cells can be related to its spectral absorption κ_λ and scattering $\sigma_{s,\lambda}$ coefficients according to (Pilon et al., 2011)

$$\bar{C}_{abs,\lambda} = \frac{\kappa_\lambda}{N_T} \quad \text{and} \quad \bar{C}_{sca,\lambda} = \frac{\sigma_{s,\lambda}}{N_T} \tag{5}$$

where N_T is the cell number density defined as the number of cells per m^3 of suspension. Alternatively, the biomass concentration of the microalgal suspension X, expressed in mass of dry weight per unit volume of suspension (g/L or kg/m^3), is often measured instead of N_T (Cornet et al., 1992; Takache et al., 2010, 2012; Kandilian et al., 2014a,b). Then, the average spectral mass absorption and scattering cross-sections $\bar{A}_{abs,\lambda}$ and $\bar{S}_{sca,\lambda}$, expressed in m^2/kg dry weight, can be expressed as

$$\bar{A}_{abs,\lambda} = \frac{\kappa_\lambda}{X} \quad \text{and} \quad \bar{S}_{sca,\lambda} = \frac{\sigma_{s,\lambda}}{X}. \tag{6}$$

Typically, the biomass concentration X in conventional PBR varies from 0.1 to 2.0 g/L (Takache et al., 2010). However, in closed intensified PBRs such as biofilm (Ozkan et al., 2012) or internally illuminated PBRs (Cornet, 2010) the biomass concentration X can reach up to 100 g/L.

2.4 Connection to Growth Kinetics and PBR Performance

From an energy point of view, the photosynthetic microorganisms "disregard" the direction of the incident photons. Then, instead of considering the directional intensity $I_\lambda(\mathbf{r}, \hat{\mathbf{s}})$, it is more appropriate to use the local spectral fluence rate $G_\lambda(\mathbf{r})$ defined as the irradiance incident from all directions, at location $\mathbf{r}$ in the PBR and expressed as

$$G_\lambda(\mathbf{r}) = \int_{4\pi} I_\lambda(\mathbf{r}, \hat{\mathbf{s}}) d\Omega. \tag{7}$$

Thanks to their different pigments, photosynthetic microorganisms can use photons with a wide variety of wavelengths. Then, the local fluence rate can be averaged over the PAR region to yield the PAR-averaged fluence rate $G_{PAR}(\mathbf{r})$ defined as (Pilon et al., 2011),

$$G_{PAR}(\mathbf{r}) = \int_{PAR} G_\lambda(\mathbf{r}) d\lambda. \tag{8}$$

Conveniently, simple analytical solutions of the RTE have been derived for $G_\lambda(\mathbf{r})$, based on the two-flux approximation, for one-dimensional flat-plate

and tubular PBRs (Cornet et al., 1992, 1995). In fact, they have been shown to predict $G_\lambda(\mathbf{r})$ and $G_{PAR}(\mathbf{r})$ accurately for outdoor open ponds and flat plate PBRs exposed to both collimated and diffuse sunlight (Lee et al., 2014). Such analytical solutions bypass the need to solve the RTE numerically. However, they still requires knowledge of the radiation characteristics of the microorganism suspensions, namely κ_λ, $\sigma_{s,\lambda}$, and b_λ.

Finally, microalgae are in suspension and move quickly through the PBR. Then, the average fluence rate G_{ave} over the entire PBR of volume V can be estimated from the local PAR-averaged fluence rate as,

$$G_{ave} = \frac{1}{V}\int_V G_{PAR}(\mathbf{r})\,dV. \tag{9}$$

The average fluence rate G_{ave} has been used in growth kinetics models such as the Haldane-type model (Andrews, 1968; Sukenik et al., 1991; Grima et al., 1996; Acien Fernandez et al., 1997; Chen et al., 2011; Béchet et al., 2013). It can be used for optically thin PBRs where the PAR-averaged fluence rate does not vary significantly within the PBR (Fernandes et al., 2010; Lee et al., 2013; Kong and Vigil, 2014). However, when the PBR features strong gradient in $G_{PAR}(\mathbf{r})$, a more general approach is to relate the local growth rate $\mu(\mathbf{r})$ to the local fluence rate $G_{PAR}(\mathbf{r})$ and average $\mu(\mathbf{r})$ over the volume of the PBR (Cornet et al., 1998; Yun and Park, 2003; Pruvost et al., 2008; Cornet and Dussap, 2009; Murphy and Berberoğlu, 2011; Takache et al., 2012; Lee et al., 2014).

An alternative approach, based on thermodynamic and biochemical considerations, consists of defining the specific local rate of photon absorption (LRPA), $\mathscr{A}$ expressed in $\mu\text{mol}_{h\nu}$/kg·s represents the amount of photons in the PAR region absorbed per unit weight of biomass and per unit time (Cornet et al., 1992; Pruvost and Cornet, 2012). The LRPA depends on the mass spectral absorption cross-section of the species and on the spectral fluence rate in the PBR. It can be expressed as (Cornet et al., 1992)

$$\mathscr{A}(\mathbf{r}) = \int_{PAR} \bar{A}_{abs,\lambda}\, G_\lambda(\mathbf{r})\,d\lambda. \tag{10}$$

It has been used to predict the growth kinetics and biomass or lipid productivities of the PBR (Pruvost and Cornet, 2012; Takache et al., 2012; Kandilian et al., 2014a).

The specific mean rate of photon absorption (MRPA) can be determined by averaging the LRPA over the volume of the PBR according to (Cornet et al., 1992)

$$\langle \mathscr{A} \rangle = \frac{1}{V} \int_V \mathscr{A}(\mathbf{r}) dV. \tag{11}$$

The MRPA $\langle \mathscr{A} \rangle$ accounts for the cumulative effects of (i) biomass concentration, (ii) the spectral mass absorption cross-section $\bar{A}_{abs,\lambda}$, and (iii) the local spectral fluence rate $G_\lambda(\mathbf{r})$ inside the PBR.

Overall, the process variables $G_{PAR}(\mathbf{r})$, G_{ave}, $\mathscr{A}(\mathbf{r})$, and $\langle \mathscr{A} \rangle$ are strongly associated with growth kinetics of microorganisms and with the productivity and efficiency of the PBRs. In order to determine these variables, it is necessary to know the radiation characteristics $\Phi_{T,\lambda}(\Theta)$, κ_λ, and $\sigma_{s,\lambda}$ of the suspension. This can be achieved numerically or experimentally, as discussed in the next sections.

3. THEORETICAL PREDICTIONS

3.1 Introduction

Theoretical predictions of the radiation characteristics $\Phi_{T,\lambda}(\Theta)$, ($\bar{C}_{abs,\lambda}$, $\bar{C}_{sca,\lambda}$) or ($\bar{A}_{abs,\lambda}$, $\bar{S}_{sca,\lambda}$) of a suspension of polydisperse photosynthetic microorganisms can be obtained by solving Maxwell's equations of electromagnetic wave theory based on the cells' shapes, size distribution, and complex index of refraction. Lorenz–Mie theory refers to the analytical solution of Maxwell's equations for homogeneous and spherical particles (Mie, 1908; Bohren and Huffman, 1998). Analytical solutions also exist for homogeneous concentric spheres or coated spheres (Aden and Kerker, 1951; Bohren and Huffman, 1998) and randomly oriented and infinitely long cylinders (Wait, 1955; Kerker, 1969; Bohren and Huffman, 1998). Note, however, that all these analytical expressions require the use of a computer program.

For more complex shapes, Maxwell's equations can be solved numerically. However, given the complexity and variations in the morphology of the photosynthetic microorganisms and despite the increasing available computing resources, simplifications of the shape and/or of the optical properties of the photosynthetic microorganisms are necessary. This section presents the different theoretical approaches used to predict the radiation characteristics of microorganisms and discusses their advantages and limitations.

3.2 Heterogeneous vs Homogeneous

Despite the heterogeneous nature of photosynthetic microorganism cells (Fig. 1), they have typically been treated as homogeneous with some effective complex index of refraction (Quirantes and Bernard, 2004; Pottier et al., 2005; Jonasz and Fournier, 2007; Berberoğlu et al., 2007; Gordon, 2011; Lee et al., 2013; Dauchet et al., 2015). This assumption can be justified by the often small mismatch in complex index of refraction between the different cell compartments. In addition, it was validated by Quirantes and Bernard (2004) who modeled single cell microalgae as homogeneous spheres and as coated spheres. The outer coating was assumed to be nonabsorbing and represented the cellular cytoplasm. By contrast, the inner core, representing the organelles and chloroplasts, was absorbing and featured a larger refractive index than the outer coating. The authors found that light absorption and scattering cross-sections of a homogeneous sphere with volume-averaged complex index of refraction were similar to those of the coated sphere for representative wavelengths, cell dimensions, and optical properties (Quirantes and Bernard, 2004).

Alternatively, one could treat microorganisms as heterogeneous cells. Advanced numerical tools can solve Maxwell's equations for very complex heterogeneous structures (Waterman, 1965; Mackowski, 1994; Mishchenko et al., 2002, 1995). However, the number of input parameters would be very large to account for the shapes, dimensions, volume fractions, and spectral complex index of refraction of the various cell compartments (e.g., nucleus, chloroplast, cell wall, mitochondria, cytoplasm, starch grains). The latter is difficult to measure *in vivo* and usually is not precisely known, in particular as a function of wavelength over the PAR region (Jonasz and Fournier, 2007). In addition, the computational cost to predict spectral radiation characteristics while accounting for the different organelles as well as the polydispersity of the cell population seems quite prohibitive for currently available computing resources. However, for some species, a compromise could be to model cells as coated spheres without adding significant complexity. For example, *Chlorella*, feature a relatively thick ($\sim$130 nm; Gerken et al., 2013) and nonabsorbing but strongly refracting ($n \sim 1.5$; Atkinson Jr et al., 1972; Traverse, 2007) cell wall that could be modeled as the coating of a homogeneous core.

3.3 Effective Optical Properties of Photosynthetic Microorganisms

Jonasz and Fournier (2007) reviewed various methods used to predict or measure (i) the average refractive index n, (ii) the spectral refractive index n_λ,

(iii) the spectral absorption index k_λ, or (iv) the complex index of refraction m_λ for phytoplankton and bacteria in water. For example, Aas (1996) used the Lorenz–Lorenz effective medium approximation (EMA) to determine n from the various components of the phytoplankton cells. The authors pointed out that uncertainty in the water content had a significant effect on the predictions, even more than the choice of EMA. Alternatively, Bricaud, Morel, and Stramski (Bricaud and Morel, 1986; Bricaud et al., 1988; Stramski et al., 2001) used the Helmholtz–Ketteler theory (Jonasz and Fournier, 2007) for n_λ and k_λ to predict the complex index of refraction of various phytoplanktons. The parameters of the model were retrieved by fitting theoretical predictions with experimental measurements of absorption spectra for various phytoplankton suspensions.

Pottier et al. (2005) predicted the radiation characteristics of *C. reinhardtii* using the Lorenz–Mie theory assuming that (i) the cells were homogeneous and spherical, (ii) the refractive index was constant over the PAR and equal to 1.55, and (iii) the absorption index was given by

$$k_\lambda = \frac{\lambda}{4\pi}\sum_j C_j Ea_j = \frac{\lambda}{4\pi}\rho_{dry}(1-x_w)\sum_j w_j Ea_j \tag{12}$$

where C_j is the concentration of j^{th} pigment in the cell (in kg/m^3) while ρ_{dry} is the density of the dry biomass (in kg/m^3), x_w is the average water mass fraction in the cells, and $w_j = C_j/X$ is the concentration of j^{th} pigment on a dry mass basis. Moreover, Ea_j (in m^2/kg) is the specific absorption cross-section of individual pigments, as reported by Bidigare et al. (1990) and reproduced in Fig. 2.

Recently, Dauchet et al. (2015) relaxed the assumption of constant refractive index. Instead, they predicted the refractive index n_λ of microalgae cells using the subtractive Kramers–Kronig relation based on the absorption index k_λ of the microorganism, estimated by Eq. (12) (Pottier et al., 2005). Then, the refractive index of the cell was estimated according to (Dauchet et al., 2015)

$$n_\nu = n_{\nu_p} + 2\frac{(\nu^2-\nu_p^2)}{\pi}P\int_{\nu_{\min}}^{\nu_{\max}}\frac{\nu' k_{\nu'}}{(\nu'^2-\nu^2)(\nu'^2-\nu_p^2)}d\nu'. \tag{13}$$

where $\nu = c/\lambda$ is the frequency of radiation, c is the speed of light in vacuum, and P is the Cauchy principal value. The anchor frequency denoted by ν_p was chosen such that the cells did not absorb at that frequency, i.e., $k_{\nu_p} = 0$. On the other hand, the value for n_{ν_p} must be known or retrieved

experimentally.Dauchet et al. (2015) chose an anchor wavelength λ_p as 820 nm for *C. reinhardtii* as green microalgae do not absorb at $\lambda \geq 750$ nm (Dauchet et al., 2015). The authors retrieved a value of $n_{\nu_p} = 1.44$ for *C. reinhardtii* using an inverse method that minimized the difference between the measured and the predicted normal–hemispherical transmittance at 820 nm. The latter was estimated by solving the RTE using the Monte Carlo method and the predicted radiation characteristics of the microorganisms.

Finally, Pilon and coworkers (Lee et al., 2013; Kandilian et al., 2013; Heng et al., 2014) retrieved the spectral complex index of refraction m_λ over the PAR region for various microalgae and cyanobacteria from the experimental measurements of their absorption and scattering cross-sections. The authors used an inverse method based on genetic algorithm and a forward method based on one of the theoretical models described in the next sections.

3.4 Radiation Characteristics of Unicellular Spheroidal Microorganisms

The radiation characteristics of axisymmetric spheroidal microorganisms, such a *C. reinhardtii* (Fig. 1A), with major and minor diameters a and b can be predicted numerically using (i) the T-matrix method (Waterman, 1965; Mackowski, 1994; Mishchenko et al., 2002, 1995), (ii) the discrete-dipole approximation (Draine, 1988), and (iii) the finite-difference time-domain method (Liou, 2002). Most often, however, they have been approximated as homogeneous spheres with some equivalent radius r_{eq} and some effective complex index of refraction $m_\lambda = n_\lambda + ik_\lambda$ (Pottier et al., 2005; Berberoğlu et al., 2007; Dauchet et al., 2015), as discussed in Section 3.6.1.

In general, the size-averaged absorption $\bar{C}_{abs,\lambda}$ and scattering $\bar{C}_{sca,\lambda}$ cross-sections of polydisperse spheroidal microalgae suspension with size distribution $f(a, b)$ can be estimated as (Pilon et al., 2011)

$$\bar{C}_{abs,\lambda} = \int_0^\infty \int_0^\infty C_{abs,\lambda}(a,b) f(a,b) da db \quad \text{and} \quad \bar{C}_{sca,\lambda} = \int_0^\infty C_{sca,\lambda}(a,b) f(a,b) da db. \tag{14}$$

Note that the same expressions apply to the mass cross-sections $\bar{A}_{abs,\lambda}$ and $\bar{S}_{sca,\lambda}$. Similarly, the total scattering phase function $\Phi_{T,\lambda}(\Theta)$ of the suspension is expressed (Modest, 2013)

$$\Phi_{T,\lambda}(\Theta) = \frac{1}{\bar{C}_{sca,\lambda}} \int_0^\infty \int_0^\infty C_{sca,\lambda}(a,b)\Phi_\lambda(a,b,\Theta) f(a,b)\, da db \qquad (15)$$

where $\Phi_\lambda(a, b, \Theta)$ is the scattering phase function of a single spheroidal scatterer with major and minor diameters a and b. Similar averaging over the cell population can be formulated for particles with other shapes as long as the geometry can be parameterized with one or more parameters.

Finally, the average absorption $\bar{C}_{abs,\lambda}$ and scattering $\bar{C}_{sca,\lambda}$ cross-sections of the suspension are related to the mass absorption $\bar{A}_{abs,\lambda}$ and scattering $\bar{S}_{sca,\lambda}$ cross-sections by (Pottier et al., 2005)

$$\bar{A}_{abs,\lambda} = \frac{\bar{C}_{abs,\lambda}}{V_{32}\rho_{dry}(1-x_w)} \quad \text{and} \quad \bar{S}_{sca,\lambda} = \frac{\bar{C}_{sca,\lambda}}{V_{32}\rho_{dry}(1-x_w)}. \qquad (16)$$

Here, V_{32} (in m^3) is the Sauter mean diameter of the cells, x_w is the average mass fraction of water in the cells, and ρ_{dry} is the density of dry material in the biomass. This relationship is often useful when comparing theoretical predictions and experimental measurements or for retrieving the effective complex index of refraction of microorganisms from the measurements of $\bar{A}_{abs,\lambda}$ and $\bar{S}_{sca,\lambda}$ (Lee et al., 2013; Heng et al., 2014). However, it requires knowledge of x_w whose measurement is often affected by large experimental uncertainty (Jonasz and Fournier, 2007).

3.5 Multicellular Microorganisms and Colonies

Several numerical methods exist to estimate the radiation characteristics of (i) multicellular microorganisms, such as filamentous cyanobacteria, and (ii) aggregates consisting of spherical cells, such as microalgae colonies. They include the superposition T-matrix method (Mackowski, 1994; Mackowski and Mishchenko, 1996, 2011; Mishchenko, 2015), the generalized multiparticle-Mie theory (Xu, 1997), and the volume integral method (Iskander et al., 1989), to name a few. The superposition T-matrix method is based on the superposition solutions of Maxwell's equations for single spherical monomers or cells. The electromagnetic (EM) field scattered by the entire aggregate of cells is the sum of the EM fields scattered by each of the constituent cells (Mackowski and Mishchenko, 1996). The EM field incident onto a monomer takes into account not only the incident EM field but also the scattered fields from all the other cells in the aggregate (Mackowski and Mishchenko, 1996). The interacting fields are transformed into a system of sphere-centered equations for the scattering coefficients and

inverted to obtain the T-matrix (Mackowski and Mishchenko, 1996). Then, the absorption and scattering cross-sections of the randomly oriented aggregate of spherical cells can be obtained from operations on the T-matrix (Mackowski and Mishchenko, 1996).

The use of the T-matrix method for nonspherical particles and for aggregates of spherical particles has been popularized by Mishchenko and Mackowski thanks to the availability of regularly updated computer programs and their user's manual (Mishchenko et al., 2002; Mackowski and Mishchenko, 2011; Mishchenko, 2015). However, depending on the number of cells and/or on the size of the aggregate, calculations can be time consuming and often require large computational resources (Kimura et al., 2003).

3.6 Equivalent Scattering Particles

Efforts have been made to approximate the radiation characteristics of (i) nonspherical unicellular microorganisms, (ii) multicellular microorganisms, and (iii) aggregates of cells with complex morphologies by those of particles with simple shapes such as spheres, coated spheres, or infinitely long cylinders. The radiation characteristics of such scatterers with simple shapes can be computed relatively rapidly (Kerker, 1969; Bohren and Huffman, 1998; Kahnert et al., 2014) compared with predictions by the T-matrix method, for example. This is particular important for real-time monitoring and control of PBRs as well as for inverse method aiming to retrieve the spectral complex index of refraction of microorganisms from their measured cross-sections (Heng et al., 2014).

3.6.1 Nonspherical Unicellular Microrganisms

As previously mentioned, nonspherical cells have been modeled as spheres with equivalent radius and effective complex index of refraction. This approximation can be justified by the fact that they are typically well mixed and randomly oriented in the PBRs. Then, the equivalent radius r_{eq} can be approximated such that either the volume or the surface area of the equivalent sphere is identical to that of the actual cell. The radius r_v of the volume-equivalent sphere can be expressed as

$$r_v = a\left(\frac{3}{2\epsilon}\right)^{1/3} \tag{17}$$

where, ϵ is the spheroid aspect ratio defined as $\epsilon = a/b$. Alternatively, the radius r_s of the surface area-equivalent sphere is given by

$$r_s = \frac{1}{4}\left(2a^2 + 2ab\frac{\sin^{-1}e}{e}\right)^{1/2} \quad \text{where} \quad e = \frac{(\epsilon^2 - 1)^{1/2}}{\epsilon}. \tag{18}$$

Lorenz–Mie theory predicts the absorption $C_{abs,\lambda}$ and scattering $C_{sca,\lambda}$ cross-sections of a single homogeneous spherical cell based on (i) the equivalent cell radius r_{eq} (e.g., r_v or r_s), (ii) the wavelength λ of interest, (iii) the refractive index $n_{m,\lambda}$ of the nonabsorbing medium at λ, and (iv) the complex index of refraction of the microorganism $m_\lambda = n_\lambda + ik_\lambda$. In fact, the cross-sections depend only on the size parameter $\chi_{eq} = 2\pi r_{eq}/\lambda$ and on the relative index of refraction $m_{r,\lambda} = m_\lambda / n_{m,\lambda}$, i.e., $C_{abs/sca,\lambda} = C_{abs/sca,\lambda}(\chi_{eq}, m_{r,\lambda})$.

In addition, the anomalous diffraction approximation can also be used to predict the cross-sections of spherical cells based on the facts that (i) their relative complex index of refraction $m_{r,\lambda}$ is such that $|m_{r,\lambda} - 1| \ll 1$ and (ii) the size parameter $\chi_{eq} = 2\pi r_{eq}/\lambda$ satisfies $\chi_{eq}|m_{r,\lambda} - 1| \ll 1$ (van de Hulst, 2012; Jonasz and Fournier, 2007). This approximation offers simple analytical expressions for the cross-sections expressed as $C_{abs/sca,\lambda} = C_{abs/sca,\lambda}(\chi_{eq}, m_{r,\lambda})$. It has been widely used in the ocean optics community to predict the radiation characteristics of phytoplanktons (Bricaud and Morel, 1986; Stramski et al., 1988; Bricaud et al., 1988; Jonasz and Fournier, 2007).

Nonspherical cells can also be easily modeled as coated spheres. For example, Quirantes and Bernard (2006) modeled *Aureococcus anophagefferens* cells as coated spheres with a shell volume fraction of 15%. The inner core and outer coating corresponded to the cytoplasm and chloroplast and their complex index of refraction was equal to 1.36 and $1.4+i0.005$, respectively. The authors compared theoretical predictions of algal bloom reflectance to measurements by a tethered surface radiometer. They found better agreement between measurements and prediction when the cells were modeled as coated spheres compared to when they were modeled as homogeneous spheres. This was attributed to the larger backscattering ratio of the coated spheres compared to homogeneous spheres of the same outer radius and effective volume-averaged complex index of refraction.

3.6.2 Multicellular Microorganisms and Colonies

Recently, Lee and Pilon (2013) demonstrated that the absorption and scattering cross-sections per unit length of randomly oriented linear chains of spheres, representative of filamentous cyanobacteria (Fig. 1D), can be approximated as those of randomly oriented infinitely long cylinders with equivalent volume per unit length. Then, for linear chains of monodisperse cells of diameter d_s, the diameter $d_{c,V}$ of the volume-equivalent infinitely

long cylinder is given by $d_{c,V} = \sqrt{2/3}d_s$. This approximation was used to retrieve the spectral complex index of refraction of *Anabeana cylindrica* over the PAR region (Heng et al., 2014).

Heng et al. (2015) demonstrated that the absorption $\bar{C}_{abs,\lambda}$ and scattering $\bar{C}_{sca,\lambda}$ cross-sections and the asymmetry factor g_λ of bispheres, quadspheres, and rings of up to 20 spherical cells could be approximated as those of coated spheres such that (i) the coating has the same total volume V_T and complex index of refraction m_λ as the cells, (ii) the inner core has the same index of refraction $n_{m,\lambda}$ as the surrounding medium, and (iii) the projected area of the equivalent coated sphere is the same as the average projected area $\bar{A}_p$ of the multicellular microorganisms. Kandilian et al. (2015) proved that this volume and average projected area equivalent coated sphere approximation can also be used for fractal aggregates of up to 1000 spherical microalgae with a wide range of size parameter and relative complex index of refraction. In fact, this approximation was able to capture the effects of both multiple scattering and shading among constituent cells on the integral radiation characteristics of the aggregates. Then, the equivalent coated sphere has inner $r_{i,V+\bar{A}_p}$ and outer $r_{o,V+\bar{A}_p}$ radii expressed as (Heng et al., 2015)

$$r_{i,V+\bar{A}_p} = \left(r_{o,V+\bar{A}_p}^3 - \frac{3}{4\pi}V_T\right)^{1/3} \quad \text{and} \quad r_{o,V+\bar{A}_p} = \left(\frac{\bar{A}_p}{\pi}\right)^{1/2} \tag{19}$$

The total volume V_T of an arbitrary aggregate made of N_s polydisperse spherical cells of radius $(r_j)_{1\le j\le N_s}$ can be written as (Heng et al., 2015)

$$V_T = \sum_{j=1}^{N_s} \frac{4\pi}{3} r_j^3 \tag{20}$$

The average projected area $\bar{A}_p$ of randomly oriented multicellular microorganisms and of colonies of spherical cells can be estimated numerically, as described in Heng et al. (2015). For monodisperse spherical cells, it was found to be proportional to the square of the constitutive cell radius r_s such that (Heng et al., 2015)

$$\bar{A}_p = \alpha(N_s) r_s^2 \tag{21}$$

where α is a constant depending on the number of cells N_s in the multicellular microbe. For bispheres and quadspheres, $\alpha(2)$ and $\alpha(4)$ were found to be equal to 5.35 and 9.70, respectively. For a circular ring of N_s monodisperse cells $\alpha(N_s)$ was such that $\alpha(N_s) = 2.42N_s$ for $N_s \ge 5$. Similarly, for

fractal aggregates, $\alpha(N_s)$ was given by $\alpha(N_s) = \pi N_s^{\gamma}$ where the exponent γ was a function of the aggregate's fractal dimension D_f. It was fitted with numerically generated data for different values of D_f varying from the limiting cases of $D_f = 1.0$ corresponding to linear chains of spheres and $D_f = 3.0$ for spheres aggregated in a simple cubic packing so that (Kandilian et al., 2015)

$$\gamma = 0.73 + 0.19\left[1 + \left(\frac{D_f - 1}{2}\right)^{1.8}\right]^{1/1.8} \tag{22}$$

Note that the coated sphere approximation can be used in other fields as different from light transfer in PBR as combustion systems (Drolen and Tien, 1987; Mengüç et al., 1994) and atmospheric science (Latimer and Wamble, 1982; Latimer, 1985). In addition, $\bar{A}_p$ can be measured using image analysis of two-dimensional micrographs of freely suspended microorganisms (Brown and Vickers, 1998).

Overall, the main challenges of the theoretical approach for predicting the radiation characteristics of photosynthetic microorganisms reside in (i) predicting accurately both their effective refractive index n_λ and the absorption index k_λ as functions of wavelength and of the cell's biochemical composition and in (ii) accounting for their complex shape and their polydispersity. To date, these challenges have not been fully addressed and/or the state of the art models have not been rigorously validated. Experimental measurements offer an alternative to determine the microorganisms' radiation characteristics without relying on assumption difficult to verify.

4. EXPERIMENTAL MEASUREMENTS

This section presents a versatile method to measure directly the complete set of radiation characteristics $\mathbf{\Phi}_{T,\lambda}(\Theta)$, and ($\bar{C}_{abs,\lambda}$, $\bar{C}_{sca,\lambda}$) or ($\bar{A}_{abs,\lambda}$, $\bar{S}_{sca,\lambda}$) of photosynthetic microorganisms of various shapes and sizes.

4.1 Assumptions

The following assumptions are necessary in the data analysis of experimental measurements: (1) the photosynthetic microorganisms are well mixed and randomly oriented. (2) For all measurements, the pathlength and cell concentration of the samples are relatively small such that single scattering prevails, i.e., photons undergo one scattering event at most as they travel through the suspension. (3) The scattering phase function $\mathbf{\Phi}_{T,\lambda}(\Theta)$ has

azimuthal symmetry and is only a function of the polar angle. This can be satisfied by ensuring that the microorganisms are randomly oriented (Jonasz and Fournier, 2007). In addition, (4) $\Phi_{T,\lambda}$ is assumed to be time invariant and constant over the PAR region. Finally, (5) the suspension is scattering in the forward direction, i.e., the scatterers are large compared with the wavelength of interest.

4.2 Scattering Phase Function

The scattering phase function $\Phi_{T,\lambda}(\Theta)$ of the microalgae can be measured using a polar nephelometer, as illustrated in Fig. 4. A typical nephelometer is comprised of a probe with a small acceptance angle such that it can measure the scattered radiation as a function of the polar angle. A laser provides a continuous beam narrowly centered around wavelength λ in the PAR region. It is modulated by a beam chopper at constant frequency. The modulated beam is collimated and reduced in size by a set of collimating lenses and a pinhole. The collimated beam enters a sample holder dish containing

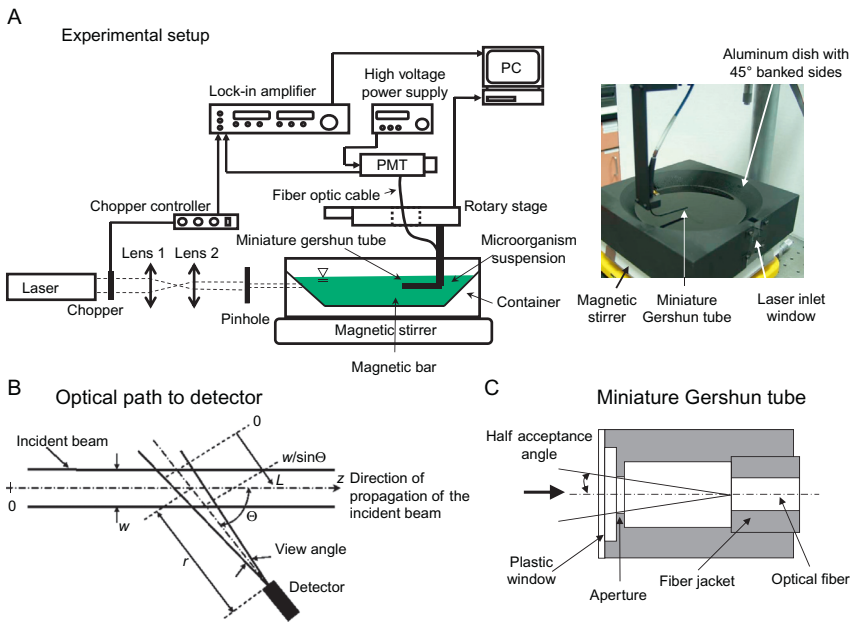

Figure 4 Schematic of (A) the nephelometer used to measure the scattering phase function at wavelength λ of the laser. (B) Optical path with coordinate system used in recovering the scattering phase function from the measured intensity distribution (Privoznik et al., 1978). (C) The miniaturized Gershun tube (drawings not to scale).

the microorganism suspension through a transparent glass window. The microorganisms are kept in suspension and randomly oriented with the aid of a black magnetic stirring bar and a magnetic stirrer. The scattered light is collected with a custom made fiber-optic probe immersed in the suspension and consisting of (i) a miniaturized Gershun tube with a small half acceptance angle and (ii) a UV–IR fiber-optic cable. The probe is mounted on a computer controlled motorized rotary stage (Fig. 4A). The collected light is detected with a photomultiplier tube (PMT) and amplified with a lock-in amplifier. The PMT is powered with a variable high voltage power supply. The latter enables the sensitivity of the PMT to be varied so that the input to the lock-in amplifier is within its detection range. Use of the lock-in amplifier together with the beam chopper enables the detection of noisy signals otherwise difficult to detect.

The nephelometer measures the scattered intensity I_λ in $\mathrm{Wm^{-2}sr^{-1}}$ as a function of the polar angle Θ. Then, the scattering phase function can be obtained based on the analysis derived by Privoznik et al. (1978) and leading to

$$\Phi_\lambda(\Theta) = \frac{2I_\lambda(\Theta)[U_\lambda(\Theta)]^{-1}}{\int_0^\pi I_\lambda(\Theta)[U_\lambda(\Theta)]^{-1}\sin\Theta d\Theta} \tag{23}$$

The geometrical correction term $U_\lambda(\Theta)$ accounts for the variation of the scattering volume and the pathlength with detection angle and is given by (Privoznik et al., 1978)

$$U_\lambda = \int_0^{w/\sin\Theta} \left(1+\beta_\lambda\frac{w}{2}c\tan\Theta-\beta_\lambda L\cos\Theta\right)\left[1-\beta_\lambda\left(r-\frac{w}{2\sin\Theta}\right)\right] \times\left[1-\beta_\lambda\left(\frac{w}{\sin\Theta}-L\right)\right]dL \tag{24}$$

where w is the beam diameter, r is the radius of rotation of the fiber-optic probe, and L is the coordinate direction along the line of sight of the detector, marking the length of the scattering volume (Fig. 4B).

Moreover, the extinction coefficient $\beta_\lambda = \kappa_\lambda + \sigma_{s,\lambda}$ of the suspension can be determined with the nephelometer by measuring the radiation flux $F_\lambda(z)$, expressed in $\mathrm{Wm^{-2}}$, at two different locations z_1 and z_2 along the path of a divergent incident beam. Then, the extinction coefficient is given by

$$\beta_\lambda = \frac{\ln|F_\lambda(z_2)/F_\lambda(z_1) + \ln(z_2^2/z_1^2)}{z_1 - z_2} \tag{25}$$

where z is the distance between the detector and the virtual image of the last lens in the optical setup.

Finally, the above measurements can be performed for different wavelengths by employing different types of lasers emitting at different wavelengths. However, there exists a limited number of options in the PAR region. Alternatively, one can assume that the scattering phase function is independent of wavelength as done in the literature for *A. variabilis* (Merzlyak and Naqvi, 2000). This has been corroborated with analysis and experimental measurements for cyanobacteria *Synechococcus* (Stramski and Mobley, 1997) and green microalgae *N. occulata* (Kandilian et al., 2013).

4.3 Absorption and Scattering Cross-Sections

The average absorption and scattering cross-sections $\bar{C}_{abs,\lambda}$ and $\bar{C}_{sca,\lambda}$ of microorganisms suspensions can be experimentally measured using a spectrometer equipped with an integrating sphere. First, the spectral normal–normal $T_{nn,\lambda}$ and normal–hemispherical $T_{nh,\lambda}$ transmissions of several dilute suspensions with different known concentrations are measured, as illustrated in Fig. 5. Here, the scattering phase function $\Phi_{T,\lambda}(\Theta)$ previously measured for the same suspension is used to correct for various optical effects.

The apparent extinction coefficient β^*_λ can be obtained from normal–normal transmittance measurements of cuvettes, of pathlength t containing either the microalgae suspension $T_{nn,\lambda,X}$ or the reference medium $T_{nn,\lambda,ref}$ (Pilon et al., 2011)

$$\beta^*_\lambda = -\frac{1}{t}\ln\left(\frac{T_{nn,\lambda,X}}{T_{nn,\lambda,ref}}\right). \tag{26}$$

Similarly, the apparent absorption coefficient κ^*_λ can be defined from the normal–hemispherical transmittance $T_{nh,\lambda}$ as (Pilon et al., 2011)

$$\kappa^*_\lambda = -\frac{1}{t}\ln\left(\frac{T_{nh,\lambda,X}}{T_{nh,\lambda,ref}}\right) \tag{27}$$

In addition, the apparent extinction coefficient β^*_λ can also be expressed as a function of the actual absorption κ_λ and scattering $\sigma_{s,\lambda}$ coefficients (Pilon et al., 2011)

$$\beta^*_\lambda = \kappa_\lambda + (1-\epsilon_n)\sigma_{s,\lambda}. \tag{28}$$

Here, ϵ_n represents the fraction of light scattered in the forward direction and detected by the spectrometer. Ideally, ϵ_n is equal to zero and $\beta^*_\lambda = \beta_\lambda$.

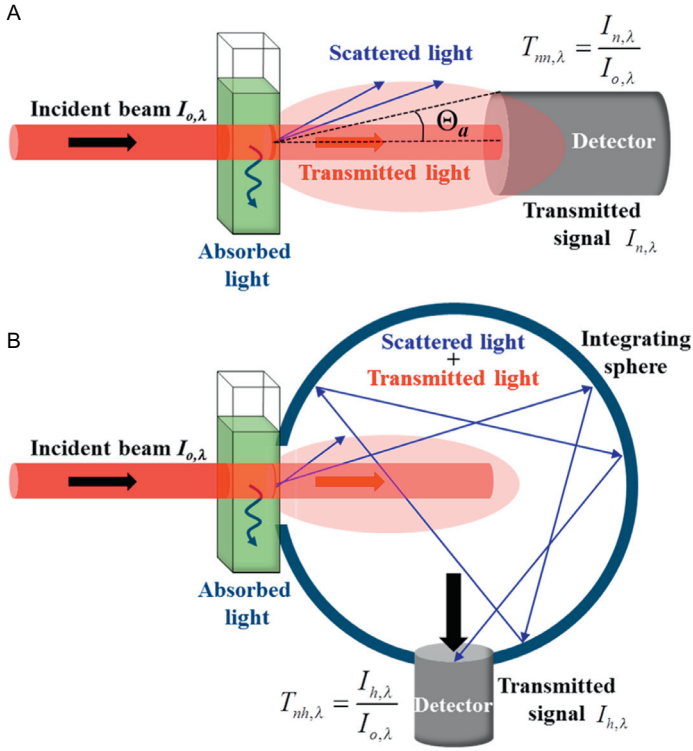

Figure 5 Schematic of experimental setup used to determine (A) the extinction coefficient β_λ from normal–normal spectral transmittance and (B) the absorption coefficient κ_λ from normal–hemispherical spectral transmittance.

However, due to the finite size of the acceptance angle of the detector, ϵ_n is larger than zero and is assumed to be constant over the PAR region. It can be defined from the suspension's scattering phase function $\Phi_{T,\lambda}(\Theta)$ previously measured as (Pilon et al., 2011)

$$\epsilon_n = \frac{1}{2}\int_0^{\Theta_a} \Phi_{T,\lambda}(\Theta)\sin\Theta d\Theta \tag{29}$$

where Θ_a is the half acceptance angle of the spectrometer's detector (Fig. 5A). The actual extinction coefficient $\beta_\lambda = \kappa_\lambda + \sigma_{s,\lambda}$ can then be determined according to

$$\beta_\lambda = \frac{\beta_\lambda^* - \epsilon_n \kappa_\lambda}{1 - \epsilon_n}. \tag{30}$$

Similarly, the apparent absorption coefficient κ_λ^* is related to the actual absorption κ_λ and scattering $\sigma_{s,\lambda}$ coefficients according to (Pilon et al., 2011)

$$\kappa_\lambda^* = \kappa_\lambda + (1-\epsilon_h)\sigma_{s,\lambda}. \tag{31}$$

Here, ϵ_h is the fraction of the scattered light detected by the detector connected to the integrating sphere. Ideally, when all the scattered light is accounted for, ϵ_h is equal to unity. Moreover, at $\lambda = 750$ nm green microalgae are assumed to be nonabsorbing, i.e., $\kappa_{750} = 0\ \mathrm{m}^{-1}$. Then, Eqs. (28) and (31) at 750 nm simplify to

$$\beta_{750}^* = (1-\epsilon_n)\sigma_{s,750} \quad \text{and} \quad \kappa_{750}^* = (1-\epsilon_h)\sigma_{s,750}. \tag{32}$$

Combining Eqs. (30) to (32) yields

$$\kappa_\lambda = \kappa_\lambda^* - \kappa_{750}^*\left(\frac{\beta_\lambda^* - \kappa_\lambda^*}{\beta_{750}^* - \kappa_{750}^*}\right) \quad \text{and} \quad \sigma_{s,\lambda} = \frac{\beta_\lambda^* - \epsilon_n\kappa_\lambda}{1-\epsilon_n} - \kappa_\lambda. \tag{33}$$

Then, the average absorption $\bar{C}_{abs,\lambda}$ and scattering $\bar{C}_{sca,\lambda}$ cross-sections of the microorganism suspension can be estimated as

$$\bar{C}_{abs,\lambda} = \kappa_\lambda / N_T \quad \text{and} \quad \bar{C}_{sca,\lambda} = \sigma_{s,\lambda}/N_T. \tag{34}$$

Similarly, κ_λ and $\sigma_{s,\lambda}$ can be divided by the samples' respective dry mass concentration X to obtain the average mass absorption and scattering cross-sections $\bar{A}_{abs,\lambda}$ and $\bar{S}_{sca,\lambda}$.

Finally, in this method, the pathlength and concentration of the samples are to be chosen such that single scattering prevails, ie, photons undergo at most one scattering event as they travel through the suspension (Assumption 1). To verify this important assumption, van de Hulst (2012) suggested that "a simple and conclusive test for the absence of multiple scattering" consists of demonstrating that the scattered intensity is directly proportional to the particle concentration. In other words, the spectral cross-sections $\bar{C}_{abs,\lambda}$ and $\bar{C}_{sca,\lambda}$ (or $\bar{A}_{abs,\lambda}$ and $\bar{S}_{sca,\lambda}$) for different values of cell density N_T (or X) should collapse onto a single line if single and independent scattering prevailed. This provides further validation of the experimental procedure and data analysis.

4.4 Validation of the Experimental Procedure

Before measuring the radiation characteristics of photosynthetic microorganisms, the experimental setups, procedures, and data analysis should be rigorously validated. To do so, experimental results for $\Phi_{T,\lambda}(\Theta)$, κ_λ, and $\sigma_{s,\lambda}$ of scatterers of known shape, size distribution, and complex index of

refraction can be compared with theoretical predictions based on the exact solution of Maxwell's equations (see Section 3). Examples of such well characterized and commercially available suspensions include polystyrene latex or glass microspheres and long glass fibers.

4.4.1 Validation of the Scattering Phase Function Measurements

Fig. 6A compares the experimentally determined scattering phase function at 632.8 nm of polystyrene latex microspheres with predictions by the Lorenz–Mie theory. The microspheres had a Gaussian size distribution of mean diameter 19 μm and standard deviation 3.56 μm. The particle complex index of refraction (in air) at 633 nm was $m_\lambda = 1.5823 + i4 \times 10^{-4}$ (Ma et al., 2003). Note that experimental measurements describe a smooth line whereas theoretical predictions show strong oscillations in $\Phi_{T,\lambda}(\Theta)$. This difference was due to the fact experimentally, the microspheres were polydisperse and in constant motion in the stirred suspension. In fact, several of them may pass by the probing volume (Fig. 4B) during the finite acquisition time of the PMT. By contrast, the theoretical predictions considered a single spherical particle of diameter 19 μm at rest in the electromagnetic (EM) field. Similarly, Fig. 6B compares the experimentally measured scattering phase function of long glass fibers and theoretical prediction for randomly oriented infinitely long cylinders of diameter 15–20 μm with complex index of refraction of $1.4567 + i\ 10^{-7}$ at 632.8 nm (Malitson, 1965; Kang et al., 2001). Similarly successful validation has been obtained with monodisperse

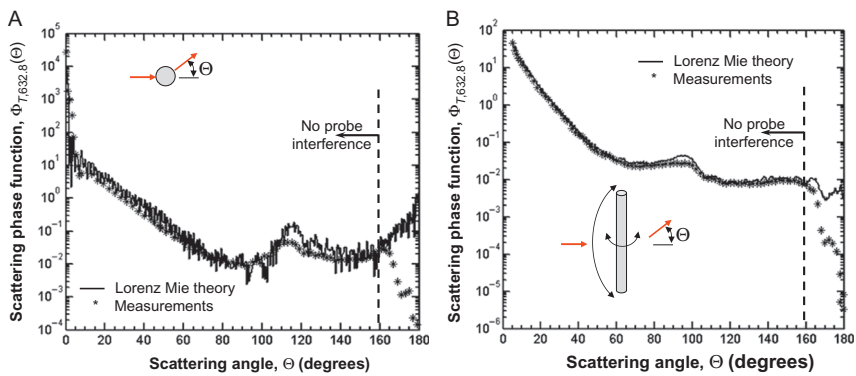

Figure 6 Comparison of the scattering phase functions at 632.8 nm measured experimentally for (A) polydisperse polystyrene latex microspheres with mean diameter 19 μm and (B) randomly oriented infinitely long glass fibers 15–20 μm in diameter along with the corresponding theoretical predictions (Berberoğlu and Pilon, 2007; Berberoğlu et al., 2008).

polystyrene latex microspheres 5 μm in diameter (Kandilian, 2014). Note that measurements beyond scattering angle of 160° should be disregarded because of the interference of the rotating fiber optic probe with the incident laser beam (Berberoğlu and Pilon, 2007). This has little consequence on the determination of the asymmetry factor g_λ since only a small amount of energy is present in these backscattering angles beyond 160° due to the large size of the microorganisms compared with the wavelength.

Overall, for both polydisperse microspheres and randomly oriented long cylinders, very good agreement was found between experimental measurements and theoretical predictions. These results demonstrate the capability of the nephelometer to measure the scattering phase function of scatterers of various shapes and sizes.

4.4.2 Validation of the Cross-Section Measurements

Fig. 7 compares the experimentally measured (A and C) absorption $\bar{C}_{abs,\lambda}$ and (B and D) scattering $\bar{C}_{sca,\lambda}$ cross-sections between 400 and 700 nm of monodisperse latex spheres 2.02 and 4.5 μm diameter with Lorenz–Mie theory predictions using the complex index of refraction of latex reported by Ma et al. (2003). Here also, the good agreement between theoretical and experimental results successfully validated the experimental setup and the data analysis. Similar validation has been performed with the same polydisperse polystyrene latex microspheres and randomly oriented and infinitely long glass fibers considered for validating the scattering phase function measurements, as illustrated in Fig. 6 (Berberoğlu and Pilon, 2007).

4.4.3 Validation of Single Scattering Assumption

Fig. 8A and B respectively show the spectral absorption κ_λ and scattering $\sigma_{s,\lambda}$ coefficients measured in the PAR region for dilute solutions of cyanobacteria *A. cylindrica* with mass concentrations X equals to 0.202, 0.296, and 0.431 kg/m^3. Each data point represents the arithmetic mean of κ_λ and $\sigma_{s,\lambda}$ measured three times for each concentration and the error bars correspond to 95% confidence interval. It is evident that the scattering and absorption coefficients increased with increasing mass concentration X. In addition, *A. cylindrica* absorbed mainly in the spectral region from 400 to 700 nm with peaks (i) at 435 and 676 nm corresponding to absorption by Chl *a* (Bidigare et al., 1990), (ii) at 630 nm corresponding to PCCN (Wolk and Simon, 1969), and (iii) a shoulder around 480 nm corresponding to absorption by PSC and PPC (Bidigare et al., 1990). In addition, scattering

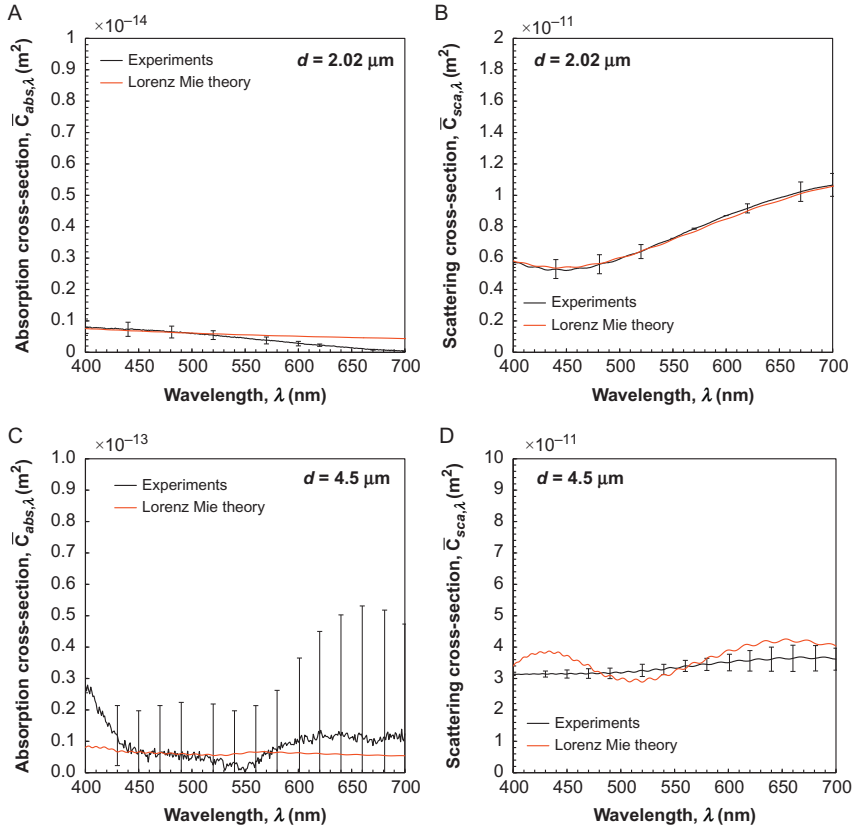

Figure 7 Experimental measurement and Lorenz–Mie theory predictions of the average absorption $\bar{C}_{abs,\lambda}$ and scattering $\bar{C}_{sca,\lambda}$ cross-sections between 400 and 700 nm of monodisperse polystyrene latex microspheres with diameters d equal to (A and B) 2.02 μm and (C and D) 4.5 μm, respectively (Kandilian, 2014).

dominated over absorption at all wavelengths between 400 and 750 nm, i.e., $\sigma_{s,\lambda} \gg \kappa_\lambda$, due to the fact that the cells were optically soft, i.e., $|m_{r,\lambda} - 1| \ll 1$.

Fig. 8C and D show the average mass absorption $\bar{A}_{abs,\lambda}$ and scattering $\bar{S}_{sca,\lambda}$ cross-sections after normalizing κ_λ and $\sigma_{s,\lambda}$ by X according to Eq. (6). It is evident that the three datasets collapsed on a single line. This confirms that single scattering prevailed and that absorption and scattering were linear processes. It is interesting to note the small dips in the scattering cross-section $\bar{S}_{sca,\lambda}$ coincided with the peaks in the absorption cross-section. This "cross-talk" between absorption and scattering can be attributed to resonance behavior in the real part (or refractive index) of the complex index of refraction of the microalgae at wavelengths when the imaginary

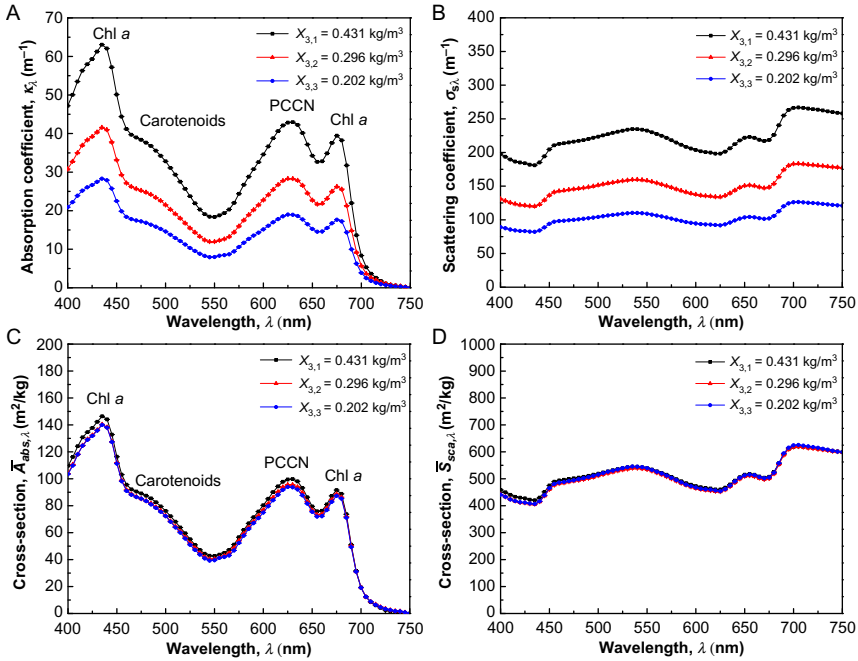

Figure 8 Experimental measurements of the (A) absorption κ_λ, and (B) scattering $\sigma_{s,\lambda}$ coefficients and of the average (C) absorption $\bar{A}_{abs,\lambda}$, and (D) scattering $\bar{S}_{sca,\lambda}$ cross-sections of dilute suspensions of *A. cylindrica* over the PAR region with different dry mass concentrations X (Heng et al., 2014).

part (or absorption index) features strong absorption peaks. Such resonance can be predicted by the Ketteler–Helmholtz theory (Jonasz and Fournier, 2007), among others.

Overall, these different results demonstrate the validity and the versatility of the described experimental method. Note that it can also be used for other absorbing and/or scattering particles as long as they can be suspended in a liquid.

5. RADIATION CHARACTERISTICS UNDER VARIOUS CONDITIONS

5.1 Exponential Growth

Experimental measurements have been performed on a wide variety of photosynthetic microorganism species. These species include (i) the green microalgae *C. reinhardtii* CC125 and its truncated chlorophyll antenna transformants tla1, tla1-CW+, and tlaX (Berberoğlu et al., 2008), (ii) the

freshwater green microalgae *Botryococcus braunii* (Berberoğlu et al., 2009) and (iii) *Chlorella* sp. (Berberoğlu et al., 2009), (iv) the marine microalgae *Chlorococcum littorale* (Berberoğlu et al., 2009) and (v) *Nannochloropsis oculata* (Kandilian et al., 2013; Heng and Pilon, 2014), (vi) the purple nonsulfur bacteria *Rhodobacter sphaeroides* (Berberoğlu and Pilon, 2007), and (vii) the filamentous cyanobacteria *Anabaena variabilis* (Berberoğlu and Pilon, 2007) and (viii) *A. cylindrica* (Heng et al., 2014). Unless otherwise noted, these measurements were performed under replete conditions during the culture's exponential growth phase. Heng and Pilon (2014) demonstrated that light transfer in PBRs can be predicted using constant radiation characteristics measured during the exponential growth phase with reasonable accuracy provided that the cultures were not nitrogen-limited. Indeed, during nitrogen starvation, pigment concentrations and radiation characteristics evolved rapidly and irreversibly with time, as discussed later in this Section.

Fig. 9 shows the scattering phase function at 632.8 nm measured experimentally for various species previously mentioned. It indicates that all these microorganisms scatter light strongly in the forward direction. In fact, in all

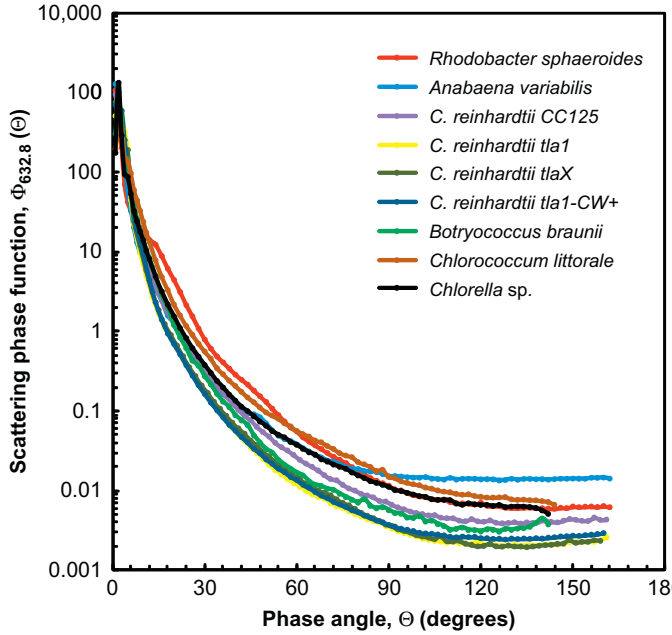

Figure 9 Scattering phase function $\Phi_{T,632.8}(\Theta)$ at 632.8 nm reported for various freshwater and marine green microalgae, cyanobacteria, and nonsulfur purple bacteria (Berberoğlu and Pilon, 2007; Berberoğlu et al., 2008, 2009; Kandilian et al., 2013).

cases, the associated asymmetry factor g_λ was larger than 0.95 and did not change significantly with wavelength (Kandilian et al., 2013).

Similarly, Fig. 10 compares the average mass spectral absorption $\bar{A}_{abs,\lambda}$ and scattering $\bar{S}_{sca,\lambda}$ cross-sections of the same species. It indicates that microorganisms presented different absorption peaks depending on the species. *C. reinhardtii* and its truncated light-harvesting antenna (tla) transformants featured absorption peaks at 435 and 676 nm corresponding to Chl *a* while the peak at 475 nm and the peak broadening around 650 nm can be attributed to Chl *b*. Note that genetic engineering led to a reduction in the absorption cross-sections across the PAR ranked by decreasing order as tla1-CW+ (with cell wall), tla1 and tlaX (without cell wall) (Berberoğlu et al., 2008). On the other hands, all *C. reinhardtii* strains had similar scattering cross-section. It is also interesting to note that filamentous cyanobacteria *A. variabilis* presented the same Chl *a* absorption peaks at 435 and 676 nm but also a peak at 621 nm corresponding to phycocyanin (PCCN) (Madigan et al., 2006). The scattering cross-section of *A. variabilis* was the largest of all microorganisms considered, most likely due to its long filaments. Finally, the nonsulfur purple bacteria *R. sphaeroides* stands out for its absorption peaks around 370, 480, 790, and 850 nm associated to the presence of bacteriochlorophyll (BChl) *b* and cartenoids (Madigan et al., 2006; Broglie et al., 1980).

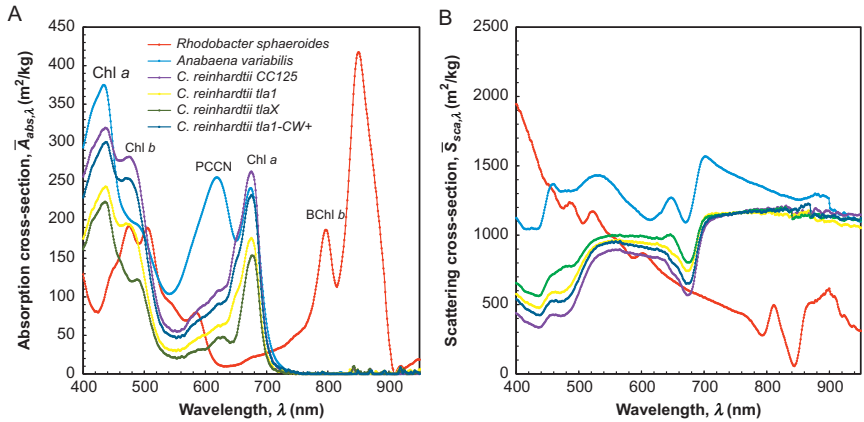

Figure 10 Average spectral mass (A) absorption $\bar{A}_{abs,\lambda}$ and (B) scattering $\bar{S}_{sca,\lambda}$ cross-sections in the spectral range from 400 to 750 nm for various green microalgae, cyanobacteria, and nonsulfur purple bacteria (Berberoğlu and Pilon, 2007; Berberoğlu et al., 2008, 2009; Kandilian et al., 2013).

The radiation characteristics shown in Figs. 9 and 10 for various species are available directly online (Pilon, 2015) or from the corresponding authors upon request.

5.2 Effect of Stresses

5.2.1 Definitions

5.2.1.1 Photoacclimation and Chromatic Acclimation

Photosynthetic microorganisms may experience photoacclimation and chromatic acclimation in response to different incident irradiance and spectrum, respectively (Fisher et al., 1996; Gentile and Blanch, 2001; Dubinsky and Stambler, 2009). Photoacclimation refers to the ability of photosynthetic microorganisms to adjust their light harvesting capacity, on the time scale of hours to days, based on the amount of light energy available to carry out photosynthesis. On the other hand, chromatic adaptation refers to the adjustment of pigment composition based on the spectral composition of the incident light.

In practice, photosynthetic microorganisms tend to increase their pigment concentrations in light-limited conditions and to reduce them under strong light illumination. For example, Fisher et al. (1996) found that *Nannochloropsis* sp. grown under 30 μmol/m^2s, in continuous cultures, had a steady-state chlorophyll concentration 4.5 times larger than when grown under 650 μmol/m^2s. Gentile and Blanch (2001) observed an 80% and 60% decrease in Chl *a* and vioxanthin, respectively, in batch grown *Nannochloropsis gaditana* when the incident irradiance was increased from 70 to 880 μmol/m^2s. However, low incident light may not always lead to significant changes in the microorganisms radiation characteristics as increasing the concentration of chlorophylls also decreases their *in vivo* specific absorption coefficient due to mutual shading of pigment molecules (Dubinsky and Stambler, 2009). The latter is partially responsible for what is known as the package effect corresponding to the nonlinear relationship between cell pigment concentrations and cell absorption cross-section (Jonasz and Fournier, 2007).

Moreover, microalgae may increase their *photoprotective* carotenoid concentration in response to large irradiance while reducing the amount of *photosynthetic* carotenoids through the so-called xanthophyll cycle (Lubián et al., 2000; Gentile and Blanch, 2001; Dubinsky and Stambler, 2009). The latter does not usually lead to changes in the overall carotenoid concentration as changes in the two types of carotenoids compensate each other (Dubinsky and Stambler, 2009; Lubián et al., 2000).

Finally, photoacclimation and chromatic acclimation depend on the microalgae species. For example, Lubián et al. (2000) demonstrated that *N. oculata* had lower concentrations of carotenoids and larger Chl *a* concentration per cell compared with *N. gaditana* and *N. salina* for cultures grown under the same conditions.

5.2.1.2 Photoinhibition

Exposing microalgae to large irradiance causes photooxidative damage in some of their photosystem units. This so-called photoinhibition leads to a decrease in the photosynthetic efficiency. This is primarily due to the destruction of reaction center proteins (Ke, 2001). The chloroplast repairs such damage by destroying the affected proteins and synthesizing new ones and integrating them into the affected photosystems. In fact, the cells continuously perform a damage repair cycle to repair the damaged photosystems (Baroli and Melis, 1996; Neidhardt et al., 1998). However, when the damage rate exceeds the repair rate, photoinhibition prevails and the overall efficiency of the cells decreases (Ke, 2001). In addition, the overall chlorophyll content can also decrease during the growth due to intense incident light. This is sometimes referred to as chlorophyll bleaching (Baroli and Melis, 1996). As a result, the absorption cross-section decreases over the PAR region and particularly at the chlorophylls absorption peaks (Fig. 2).

5.2.1.3 Nitrogen Starvation

Several strategies can be used to enhance microalgal lipid productivity (Williams and Laurens, 2010). For example, nitrogen starvation triggers large amounts of neutral lipid accumulation in various species mainly in the form of triglyceride fatty acids (TAGs) (Hu et al., 2008; Van Vooren et al., 2012). The latter are believed to serve as carbon and energy storage compound for the cells (Hu et al., 2008). TAGs are also the main feedstock for lipid to biodiesel conversion through transesterification reaction with methanol to produce methyl esters of fatty acids that are essentially biodiesel (Chisti, 2007). Kandilian et al. (2014a) demonstrated that TAG synthesis and productivity from microalgae *N. oculata* was limited by the mean rate of photon absorption $\langle \mathscr{A} \rangle$ (Eq. (11)) in the PBR during nitrogen starvation.

Nitrogen starvation can be achieved by either sudden or progressive starvation. *Sudden starvation* consists of two steps: first, microalgae are grown in nitrogen replete conditions. Then, they are transferred into a nitrogen-free medium. *Progressive starvation* consists of initially adding a small amount of nitrogen to the culture medium, in the form of nitrate, for example.

After inoculating the PBR, the microalgae grow and multiply until they consume all the nitrates in the medium and the culture medium becomes deprived of nitrogen.

In general, nitrogen limitation results in a decrease in pigment concentrations and in a significant change of color of the suspension (Kandilian et al., 2014a). In addition, the cells increase their carotenoid to Chl *a* concentration ratio (Heath et al., 1990). This ratio is related to the so-called stress index defined as the ratio of the optical densities (OD) of the cells' pigment extract at wavelengths 480 and 665 nm (Heath et al., 1990). It is an indicator of the "nutrient status" of the cells and is inversely correlated to the C/N ratio of the cells (Heath et al., 1990). In fact, Flynn et al. (1993) reported that nitrogen replete *N. oculata* cells had a carbon to nitrogen ratio (C/N) of 6 while NH_4^+ deprived cells featured C/N ratio of nearly 26 (Flynn et al., 1993).

5.2.2 Photoacclimation and Progressive Nitrogen Starvation

Fig. 11A and B presents the average spectral absorption cross-sections $\bar{C}_{abs,\lambda}$ of *N. oculata* at different times during their growth in a flat-plate PBR operated in batch mode under 7500 and 10,000 lux, respectively (Heng and Pilon, 2014). The incident light was provided by red LEDs emitting at 630 nm. The average absorption cross-section $\bar{C}_{abs,\lambda}$ displayed peaks at 435, 630, and 676 nm corresponding to *in vivo* absorption peaks of Chl *a* and at 485 nm corresponding to that of carotenoids. It also varied significantly with time in response to changes in light and nutrients availability. Similar trends were observed for both incident irradiances.

Fig. 11C and D plots $\bar{C}_{abs,\lambda}$ at wavelengths 485 and 676 nm with respect to time. Similarly, Fig. 11E and F shows the measured Chl *a* and total carotenoids (PSC + PPC) concentrations as functions of time. It is evident that the trends in the absorption peaks $\bar{C}_{abs,676}$ and $\bar{C}_{abs,485}$ closely follow the trends in Chl *a* and PSC + PPC concentrations, respectively. In fact, $\bar{C}_{abs,676}$ and $\bar{C}_{abs,485}$ and the corresponding pigment concentration reach their maximum and minimum at the same times. The initial downregulation of pigments was caused by exposure to excessive amounts of light when the cell concentration was relatively small. It contributed to reducing the energy absorbed per cell in order to prevent photodamage to their light-harvesting antenna. It is interesting to note that the duration of the initial downregulation of pigments closely coincided with the duration of the lag phase observed in the growth curves (see Fig. 2 of Heng and

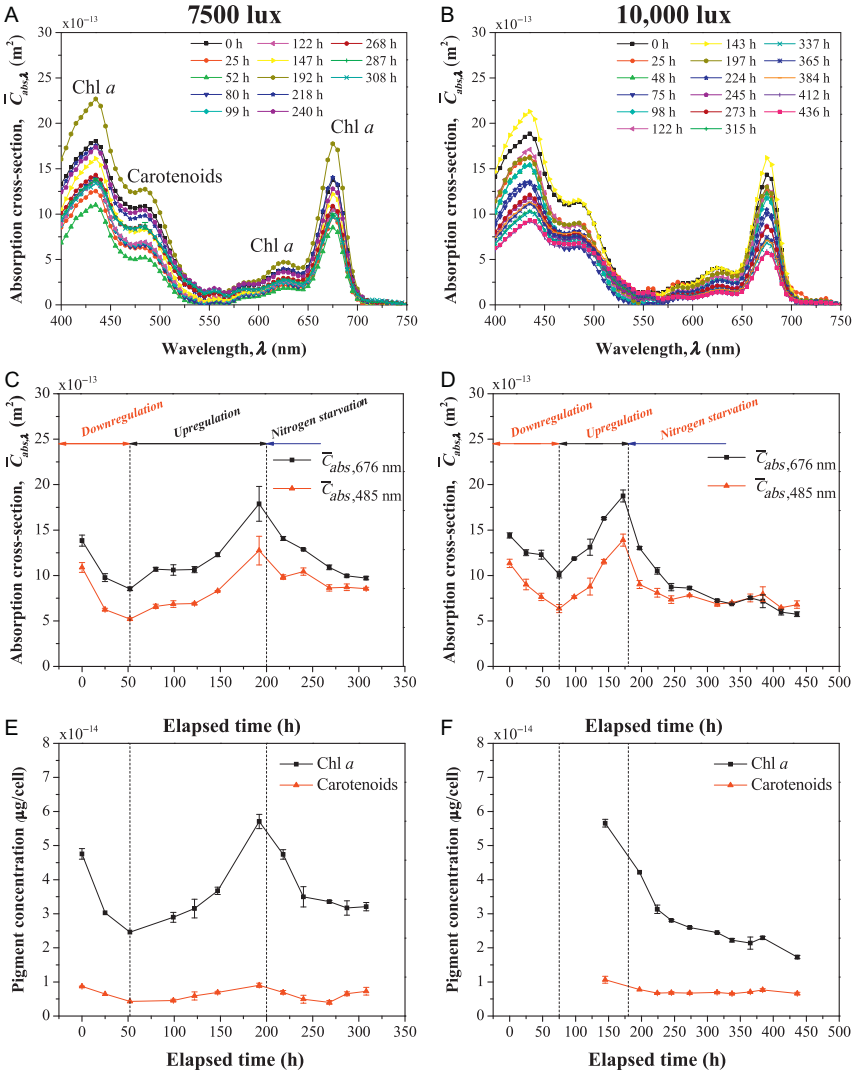

Figure 11 (A and B) Average spectral absorption cross-section $\bar{C}_{abs,\lambda}$ of *N. oculata*, (C and D) temporal evolutions (C and D) of average absorption cross-sections at 485 and 676 nm, and (E and F) of pigment Chl *a* and carotenoids for *N. oculata* grown under 7500 and 10,000 lux, respectively (Heng and Pilon, 2014).

Pilon, 2014). Then, Chl *a* and carotenoids concentrations increased between times 50 and 200 h for the culture grown under 7500 lux and between 75 and 180 h for those grown under 10,000 lux. This was due to upregulation of pigments by microalgae during the exponential growth

phase to avoid photolimitation. Finally, elemental analysis predicted that the cultures grown under 7500 and 10,000 lux became nitrogen-limited after about 200 and 180 h, respectively. Interestingly, Fig. 11E and F shows that pigment concentrations decreased sharply around those times.

5.2.3 Sudden Nitrogen Starvation

Fig. 12A and B shows the temporal evolution of the average mass absorption $\bar{A}_{abs,\lambda}$ and scattering $\bar{S}_{sca,\lambda}$ cross-sections over the PAR region for *N. oculata* during sudden nitrogen starvation of a batch culture with an initial biomass concentration X_0 of 0.23 kg/m^3 (Kandilian et al., 2014a). It illustrates how $\bar{A}_{abs,\lambda}$ decreased sharply by nearly one order of magnitude across the PAR region within 96 h. This was accompanied by a decrease in Chl *a* concentration from 3–3.5 to 0.25–0.75 wt.% and in carotenoid from 0.45–0.6 to 0.1–0.2 wt.% over the same time period (Kandilian et al., 2014a). The stress index also increased continuously during that time, as did the TAG concentration from 5–10 to 30–45 wt.% (Kandilian et al., 2014a). On the other hand, Fig. 12B indicates that the scattering cross-section $\bar{S}_{sca,\lambda}$ did not change significantly during sudden nitrogen starvation. Using these radiation characteristics, Kandilian et al. (2014a) demonstrated that (i) TAG productivity correlated with light absorption rate by cells and (ii) a critical light absorption rate was needed to achieve large TAG accumulation.

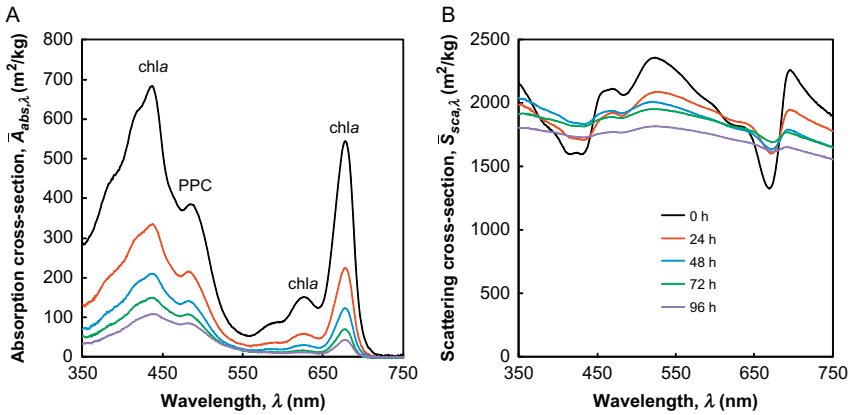

Figure 12 Average mass (A) absorption and (B) scattering cross-sections of *N. oculata* after 0, 24, 48, 72, and 96 h of cultivation during sudden nitrogen starvation of batch culture exposed to 250 μmol$_{h\nu}$/m^2 s with initial biomass concentration $X_0 = 0.23$ kg/m^3.

6. CONCLUSIONS AND PROSPECTS

This chapter has emphasized the importance of understanding and quantifying the interaction between light and photosynthetic microorganisms in designing, optimizing, monitoring, and operating PBRs of all sizes for the production of value-added products. To do so, knowing the radiation characteristics of photosynthetic microorganisms and their evolution with time and various stresses is essential. In fact, they are directly related to growth kinetics and to lipid production. This chapter has presented theoretical and experimental methods to determine the radiation characteristics of a wide variety of promising microorganism species with various shapes, sizes, and responses to stresses.

First, the theoretical methods for predicting the radiation characteristics of photosynthetic microorganisms are relatively fast and could be used for simulating microalgae growth under various operating conditions. It could also be employed for real-time monitoring and model-based control of PBRs to achieve their maximum productivity. However, existing models make simplifications on the shape of the cells or may require several input parameters difficult to obtain in practice in order to predict the spectral complex index of refraction. In fact, they have only been validated indirectly by considering the normal–hemispherical transmittance measurements of *Chlamydomonas reinhardtii* suspension grown under optimal conditions (Pottier et al., 2005; Dauchet et al., 2015). Therefore, one should perform direct comparison between experimental measurements and numerical predictions of the radiation characteristics and of the effective complex index of refraction for selected representative microalgae grown under various conditions. To do so, their size distribution, pigment concentrations, cell composition, and radiation characteristics should be measured simultaneously.

On a more fundamental level, contradicting arguments appear in the literature on the validity of approximating cells as homogeneous (Quirantes and Bernard, 2004, 2006). In particular, it remains unclear (i) how the chloroplast spatial distribution within the cell affects its absorption cross-section, (ii) how to accurately model the package effect, (iii) how the cell organelles participate to light scattering, and (iv) how this should be accounted for. Addressing these questions is made even more difficult by the fact that "very little is known about the optical properties of these organelles" (Jonasz and Fournier, 2007). Experimental determination of *in vivo* organelles' optical properties present major challenges. However, it could ultimately help

determine the conditions under which microorganisms could be treated as homogeneous with some effective optical properties.

Moreover, the experimental measurements presented in Section 4 can faithfully capture the effect of the microorganisms' size, shape, and polydispersity. However, the experimental setup can be costly and the experimental procedure is time consuming. Thus, it may be difficult to implement in actual production systems. In addition, measurements are valid only for specific growth conditions and need to be repeated each time conditions change including pH, temperature, illumination, medium composition, etc. Thus, it would be beneficial to develop a simplified experimental method to determine the radiation characteristics and in particular the absorption cross-section which is the most influence on light transfer in PBRs (Kandilian, 2014).

Finally, many photosynthetic microorganisms have highly nonspherical and sometimes very complex shapes such as *Scenedesmus*, *Spirunila*, or *Golenkinia*. Similarly, many genus or species of interest are colonial (e.g., *Scenedesmus*, *Botryococcus*) forming complex and sometimes large colonies. Experimental measurements and theoretical methods or approximations to determine their radiation characteristics are still lacking, for the most part.

REFERENCES

Aas E: Refractive index of phytoplankton derived from its metabolite composition, *J Plankton Res* 18(12):2223–2249, 1996.

Acien Fernandez FG, Garcia Camacho F, Sanchez Perez JA, Fernandez Sevilla JM, Molina Grima E: A model for light distribution and average solar irradiance inside outdoor tubular photobioreactors for the microalgal mass culture, *Biotechnol Bioeng* 55(5):701–714, 1997.

Aden AL, Kerker M: Scattering of electromagnetic waves from two concentric spheres, *J Appl Phys* 22(10):1242–1246, 1951.

Andrews JF: A mathematical model for the continuous culture of microorganisms utilizing inhibitory substrates, *Biotechnol Bioeng* 10(6):707–723, 1968.

Atkinson AW Jr, Gunning BES, John PCL: Sporopollenin in the cell wall of *Chlorella* and other algae: ultrastructure, chemistry, and incorporation of 14C-acetate, studied in synchronous cultures, *Planta* 107(1):1–32, 1972.

Baroli I, Melis A: Photoinhibition and repair in *Dunaliella salina* acclimated to different growth irradiances, *Planta* 198(4):640–646, 1996.

Bayona KCD, Garcés LA: Effect of different media on exopolysaccharide and biomass production by the green microalga *Botryococcus braunii*, *J Appl Phycol* 26(5):2087–2095, 2014.

Béchet Q, Shilton A, Guieysse B: Modeling the effects of light and temperature on algae growth: state of the art and critical assessment for productivity prediction during outdoor cultivation, *Biotechnol Adv* 31(8):1648–1663, 2013.

Becker EW: *Microalgae: biotechnology and microbiology,* Cambridge, UK, 1994, Cambridge University Press.

Benemann JR: Production of nitrogen fertilizer with nitrogen-fixing blue-green algae, *Enzym Microb Technol* 1(2):83–90, 1979.

Benemann JR: Hydrogen production by microalgae, *J Appl Phycol* 12:291–300, 2000.

Berberoğlu H, Gomez PS, Pilon L: Radiation characteristics of *Botryococcus braunii*, *Chlorococcum littorale*, and *Chlorella* sp. used for fixation and biofuel production, *J Quant Spectrosc Radiat Transf* 110(17):1879–1893, 2009.
Berberoğlu H, Pilon L: Experimental measurement of the radiation characteristics of *Anabaena variabilis* ATCC 29413-U and *Rhodobacter sphaeroides* ATCC 49419, *Int J Hydrog Energy* 32(18):4772–4785, 2007.
Berberoğlu H, Pilon L, Melis A: Radiation characteristics of *Chlamydomonas reinhardtii* CC125 and its truncated chlorophyll antenna transformants *tla1, tlaX* and *tla1-CW+*, *Int J Hydrog Energy* 33(22):6467–6483, 2008.
Berberoğlu H, Yin J, Pilon L: Light transfer in bubble sparged photobioreactors for H_2 production and CO_2 mitigation, *Int J Hydrog Energy* 32(13):2273–2285, 2007.
Berman-Frank I, Lundgren P, Falkowski P: Nitrogen fixation and photosynthetic oxygen evolution in cyanobacteria, *Res Microbiol* 154(3):157–164, 2003.
Bidigare R, Ondrusek M, Morrow J, Kiefer D: *In vivo* absorption properties of algal pigments, *Proc SPIE Ocean Opt X* 1302:290–301, 1990.
Blankenship RE: *Molecular mechanisms of photosynthesis,* Hoboken, NJ, 2008, Wiley-Blackwell.
Bohren CF, Huffman DR: *Absorption and scattering of light by small particles,* New York, NY, 1998, John Wiley & Sons.
Bricaud A, Bédhomme AL, Morel A: Optical properties of diverse phytoplanktonic species: experimental results and theoretical interpretation, *J Plankton Res* 10(5):851–873, 1988.
Bricaud A, Morel A: Light attenuation and scattering by phytoplanktonic cells: a theoretical modeling, *Appl Opt* 25(4):571–580, 1986.
Broglie RM, Hunter CN, Delepelaire P, Niederman RA, Chua NH, Clayton RK: Isolation and characterization of the pigment-protein complexes of *Rhodopseudomonas sphaeroides* by lithium dodecyl sulfate/polyacrylamide gel electrophoresis, *Proc Natl Acad Sci* 77(1):87–91, 1980.
Brown DJ, Vickers GT: The use of projected area distribution functions in particle shape measurement, *Powder Technol* 98(3):250–257, 1998.
Canter-Lund H, Lund JWG: *Freshwater algae: their microscopic world explored,* Somerset, UK, 1995, Biopress Limited.
Chen X, Goh QY, Tan W, Hossain I, Chen WN, Lau R: Lumostatic strategy for microalgae cultivation utilizing image analysis and chlorophyll *a* content as design parameters, *Bioresour Technol* 102(10):6005–6012, 2011.
Chisti Y: Biodiesel from microalgae, *Biotechnol Adv* 25(3):294–306, 2007.
Cohen Z: *Chemicals from microalgae,* London, UK, 1999, Taylor & Francis.
Cornet JF: Calculation of optimal design and ideal productivities of volumetrically lightened photobioreactors using the constructal approach, *Chem Eng Sci* 65(2):985–998, 2010.
Cornet JF, Dussap CG: A simple and reliable formula for assessment of maximum volumetric productivities in photobioreactors, *Biotechnol Prog* 25(2):424–435, 2009.
Cornet JF, Dussap CG, Dubertret G: A structured model for simulation of cultures of the cyanobacterium *Spirulina platensis* in photobioreactors: I. Coupling between light transfer and growth kinetics, *Biotechnol Bioeng* 40(7):817–825, 1992.
Cornet JF, Dussap CG, Gros JB: Kinetics and energetics of photosynthetic micro-organisms in photobioreactors. In *Bioprocess and algae reactor technology, apoptosis*, vol. 59, Advances in Biochemical Engineering Biotechnology, Berlin, 1998, Springer, pp 153–224.
Cornet JF, Dussap CG, Gros JB, Binois C, Lasseur C: A simplified monodimensional approach for modeling coupling between radiant light transfer and growth kinetics in photobioreactors, *Chem Eng Sci* 50(9):1489–1500, 1995.
Das D, Veziroğlu TN: Hydrogen production by biological processes: a survey of literature, *Int J Hydrog Energy* 26(1):13–28, 2001.

Dauchet J, Blanco S, Cornet JF, Fournier R: Calculation of the radiative properties of photosynthetic microorganisms, *J Quant Spectrosc Radiat Transf* 161:60–84, 2015.
Dayananda C, Sarada R, Rani MU, Shamala TR, Ravishankar GA: Autotrophic cultivation of *Botryococcus braunii* for the production of hydrocarbons and exopolysaccharides in various media, *Biomass Bioenergy* 31(1):87–93, 2007.
Demura M, Ioki M, Kawachi M, Nakajima N, Watanabe M: Desiccation tolerance of *Botryococcus braunii* (trebouxiophyceae, chlorophyta) and extreme temperature tolerance of dehydrated cells, *J Appl Phycol* 26(1):49–53, 2014.
Draine BT: The discrete-dipole approximation and its application to interstellar graphite grains, *Astrophys J* 333:848–872, 1988.
Drolen BL, Tien CL: Absorption and scattering of agglomerated soot particulate, *J Quant Spectrosc Radiat Transf* 37(5):433–448, 1987.
Dubinsky Z, Stambler N: Photoacclimation processes in phytoplankton: mechanisms, consequences, and applications, *Aquat Microb Ecol* 56:163–176, 2009.
Fernandes BD, Dragone GM, Teixeira JA, Vicente AA: Light regime characterization in an airlift photobioreactor for production of microalgae with high starch content, *Appl Biochem Biotechnol* 0273-2289. 161(1-8):218–226, 2010.
Fisher T, Minnaard J, Dubinsky Z: Photoacclimation in the marine alga *Nannochloropsis* sp. (eustigmatophyte): a kinetic study, *J Plankton Res* 18(10):1797–1818, 1996.
Flynn KJ, Davidson K, Cunningham AJ: Relations between carbon and nitrogen during growth of *Nannochloropsis oculata* (droop) Hibberd under continuous illumination, *New Phytol* 125(4):717–722, 1993.
Gentile MP, Blanch HW: Physiology and xanthophyll cycle activity of *Nannochloropsis gaditana*, *Biotechnol Bioeng* 75(1):1–12, 2001.
Gerken HG, Donohoe B, Knoshaug EP: Enzymatic cell wall degradation of *Chlorella vulgaris* and other microalgae for biofuels production, *Planta* 237(1): 239–253, 2013.
Gordon HR: Light scattering and absorption by randomly-oriented cylinders: dependence on aspect ratio for refractive indices applicable for marine particles, *Opt Express* 19(5):4673–4691, 2011.
Grima EM, Sevilla JMF, Perez JAS, Camacho FG: A study on simultaneous photolimitation and photoinhibition in dense microalgal cultures taking into account incident and averaged irradiances, *J Biotechnol* 45:59–69, 1996.
Heath MR, Richardson K, Kiørboe T: Optical assessment of phytoplankton nutrient depletion, *J Plankton Res* 12(2):381–396, 1990.
Heng RL, Lee E, Pilon L: Radiation characteristics and optical properties of filamentous cyanobacterium *Anabaena cylindrica*, *J Opt Soc Am A* 31(4):836–845, 2014.
Heng RL, Pilon L: Time-dependent radiation characteristics of *Nannochloropsis oculata* during batch culture, *J Quant Spectrosc Radiat Transf* 144:154–163, 2014.
Heng RL, Sy KC, Pilon L: Absorption and scattering by bispheres, quadspheres, and circular rings of spheres and their equivalent coated spheres, *J Opt Soc Am A* 32(1):46–60, 2015.
Hu Q, Sommerfeld M, Jarvis E, et al: Microalgal triacylglycerols as feedstocks for biofuel production: perspectives and advances, *Plant J* 54(4):621–639, 2008.
Iskander MF, Chen HY, Penner JE: Optical scattering and absorption by branched chains of aerosols, *Appl Opt* 28(15):3083–3091, 1989.
Jonasz M, Fournier G: *Light scattering by particles in water: theoretical and experimental foundations,* San Diego, CA, 2007, Academic Press.
Kahnert M, Nousiainen T, Lindqvist H: Review: model particles in atmospheric optics, *J Quant Spectrosc Radiat Transf* 146:41–58, 2014.
Kandilian R: *Optimization and control of light transfer in photobioreactors for biofuel production,* Ph.D. thesis, Los Angeles, USA, 2014, University of California.

Kandilian R, Heng RL, Pilon L: Absorption and scattering by fractal aggregates and by their equivalent coated spheres, *J Quant Spectrosc Radiat Transf* 151:310–326, 2015.
Kandilian R, Lee E, Pilon L: Radiation and optical properties of *Nannochloropsis oculata* grown under different irradiances and spectra, *Bioresour Technol* 137:63–73, 2013.
Kandilian R, Pruvost J, Legrand J, Pilon L: Influence of light absorption rate by *Nannochloropsis oculata* on triglyceride production during nitrogen starvation, *Bioresour Technol* 163:308–319, 2014a.
Kandilian R, Tsao TC, Pilon L: Control of incident irradiance on a batch operated flat-plate photobioreactor, *Chem Eng Sci* 119:99–108, 2014b.
Kang RJ, Shi DJ, Cong W, Cai ZL, Ouyang F: Dispersion of the optical constants of quartz and polymethyl methacrylate glasses, *Opt Commun* 188:129–139, 2001.
Ke B: Photosynthesis: photobiochemistry and photobiophysics, *Advances in Photosynthesis,* Dordrecht, The Netherlands, 2001, Kluwer Academic Publishers.
Kerker M: *The scattering of light, and other electromagnetic radiation,* New York, NY, 1969, Academic Press.
Kimura H, Kolokolova L, Mann I: Optical properties of cometary dust: constraints from numerical studies on light scattering by aggregate particles, *Astron Astrophys* 407(1): L5–L8, 2003.
Kong B, Vigil RD: Simulation of photosynthetically active radiation distribution in algal photobioreactors using a multidimensional spectral radiation model, *Bioresour Technol* 158:141–148, 2014.
Kumar K, Dasgupta CN, Nayak B, Lindblad P, Das D: Development of suitable photobioreactors for CO_2 sequestration addressing global warming using green algae and cyanobacteria, *Bioresour Technol* 102(8):4945–4953, 2011.
Latimer P: Experimental tests of a theoretical method for predicting light scattering by aggregates, *Appl Opt* 24(19):3231–3239, 1985.
Latimer P, Wamble F: Light scattering by aggregates of large colloidal particles, *Appl Opt* 21(13):2447–2455, 1982.
Lee AK, Lewis DM, Ashman PJ: Microbial flocculation, a potentially low-cost harvesting technique for marine microalgae for the production of biodiesel, *J Appl Phycol* 21(5):559–567, 2009.
Lee E, Heng RL, Pilon L: Spectral optical properties of selected photosynthetic microalgae producing biofuels, *J Quant Spectrosc Radiat Transf* 114:122–135, 2013.
Lee E, Pilon L: Absorption and scattering by long and randomly oriented linear chains of spheres, *J Opt Soc Am A* 30(9):1892–1900, 2013.
Lee E, Pruvost J, He X, Munipalli R, Pilon L: Design tool and guidelines for outdoor photobioreactors, *Chem Eng Sci* 106:18–29, 2014.
Liou KN: *An introduction to atmospheric radiation,* Waltham, MA, 2002, Academic Press.
Lubián LM, Montero O, Moreno-Garrido I, et al: *Nannochloropsis* (eustigmatophyceae) as source of commercially valuable pigments, *J Appl Phycol* 12:249–255, 2000.
Ma X, Lu JQ, Brock RS, Jacobs KM, Yang P, Hu HH: Determination of complex refractive index of polystyrene microspheres from 370 to 1610 nm, *Phys Med Biol* 48:4165–4172, 2003.
Mackowski DW: Calculation of total cross sections of multiple-sphere clusters, *J Opt Soc Am A* 11(11):2851–2861, 1994.
Mackowski DW, Mishchenko MI: Calculation of the T-matrix and the scattering matrix for ensembles of spheres, *J Opt Soc Am A* 13(11):2266–2278, 1996.
Mackowski DW, Mishchenko MI: A multiple sphere T-matrix Fortran code for use on parallel computer clusters, *J Quant Spectrosc Radiat Transf* 112(13):2182–2192, 2011.
Madigan MT, Martinko JM: *Biology of microorganisms,* Upper Saddle River, NJ, 2006, Pearson Prentice Hall.

Madigan MT, Martinko JM, Parker J, Brock TD: *Biology of microorganisms,* Upper Saddle River, NJ, 2006, Pearson Prentice Hall.
Malitson IH: Interspecimen comparison of the refractive index of fused silica, *J Opt Soc Am* 55(10):1205–1209, 1965.
Melis A: Green alga hydrogen production: process, challenges and prospects, *Int J Hydrog Energy* 27:1217–1228, 2002.
Mengüç MP, Manickavasagam S, D'Sa DA: Determination of radiative properties of pulverized coal particles from experiments, *Fuel* 73(4):613–625, 1994.
Merzlyak MN, Naqvi KR: On recording the true absorption spectrum and scattering spectrum of a turbid sample: application to cell suspensions of cyanobacterium *Anabaena variabilis*, *J Photochem Photobiol B Biol* 58:123–129, 2000.
Mie G: Beiträge zur Optik trüber Medien, speziell kolloidaler Metallösungen, *Ann Phys* 25(3):377–445, 1908.
Mishchenko MI: *Electromagnetic scattering by particles and surfaces,* 2015. http://www.giss.nasa.gov/staff/mmishchenko/t_matrix.html.
Mishchenko MI, Mackowski DW, Travis LD: Scattering of light by bispheres with touching and separated components, *Appl Opt* 34(21):4589–4599, 1995.
Mishchenko MI, Travis LD, Lacis AA: *Scattering, absorption, and emission of light by small particles,* Cambridge, UK, 2002, Cambridge University Press.
Modest M: *Radiative heat transfer,* ed 3, Oxford, UK, 2013, Elsevier.
Murphy TE, Berberoğlu H: Effect of algae pigmentation on photobioreactor productivity and scale-up: a light transfer perspective, *J Quant Spectrosc Radiat Transf* 112(18): 2826–2834, 2011.
Nakajima Y, Ueda R: Improvement of photosynthesis in dense microalgal suspension by reduction of light harvesting pigments, *J Appl Phycol* 9(6):503–510, 1997.
Nakajima Y, Ueda R: The effect of reducing light-harvesting pigment on marine microalgal productivity, *J Appl Phycol* 12(3-5):285–290, 2000.
Neidhardt J, Benemann JR, Zhang L, Melis A: Photosystem-II repair and chloroplast recovery from irradiance stress: relationship between chronic photoinhibition, light-harvesting chlorophyll antenna size and photosynthetic productivity in *Dunaliella salina* (green algae), *Photosynth Res* 56:175–184, 1998.
Ozkan A, Kinney K, Katz L, Berberoğlu H: Reduction of water and energy requirement of algae cultivation using an algae biofilm photobioreactor, *Bioresour Technol* 114:542–548, 2012.
Pilon L: *Radiation characteristics of microalgae for CO_2 fixation and biofuel production,* 2015. http://www.seas.ucla.edu/pilon/downloads.htm.
Pilon L, Berberoğlu H, Kandilian R: Radiation transfer in photobiological carbon dioxide fixation and fuel production by microalgae, *J Quant Spectrosc Radiat Transf* 112(17):2639–2660, 2011.
Pilon L, Berberoğlu H: Chap. 11: Photobiological hydrogen production. In Sherif SA, Goswami DY, Stefanakos EKL, Steinfeld A, editors: *Handbook of hydrogen energy*, Boca-Raton, FL, 2014, CRC Press, pp 369–418.
Pinho MG, Kjos M, Veening JW: How to get (a) round: mechanisms controlling growth and division of coccoid bacteria, *Nat Rev Microbiol* 11(9):601–614, 2013.
Polle JE, Kanakagiri SD, Melis A: tla1, a DNA insertional transformant of the green alga *Chlamydomonas reinhardtii* with a truncated light-harvesting chlorophyll antenna size, *Planta* 217:49–59, 2003.
Pottier L, Pruvost J, Deremetz J, Cornet JF, Legrand J, Dussap CG: A fully predictive model for one-dimensional light attenuation by *Chlamydomonas reinhardtii* in a torus photobioreactor, *Biotechnol Bioeng* 91(5):569–582, 2005.
Privoznik KG, Daniel KJ, Incropera FP: Absorption, extinction and phase function measurements for algal suspensions of *Chlorella pyrenoidosa*, *J Quant Spectrosc Radiat Transf* 20(4):345–352, 1978.

Pruvost J, Cornet JF: Knowledge models for engineering and optimization of photobioreactors. In Posten C, Walter C, editors: *Microalgal biotechnology*, Berlin, Germany, 2012, Walter De Gruyter, pp 181–224.
Pruvost J, Cornet JF, Legrand J: Hydrodynamics influence on light conversion in photobioreactors: an energetically consistent analysis, *Chem Eng Sci* 63(14):3679–3694, 2008.
Pruvost J, Cornet JF, Pilon L: Large scale production of algal biomass: photobioreactors. In Chisti Y, Bux F, editors: *Algae biotechnology: products and processes*, UK, 2014, Springer.
Quirantes A, Bernard S: Light scattering by marine algae: two-layer spherical and nonspherical models, *J Quant Spectrosc Radiat Transf* 89(1):311–321, 2004.
Quirantes A, Bernard S: Light-scattering methods for modelling algal particles as a collection of coated and/or nonspherical scatterers, *J Quant Spectrosc Radiat Transf* 100(1-3):315–324, 2006.
Richmond A: *Handbook of microalgal culture: biotechnology and applied phycology,* Oxford, UK, 2004, Blackwell Science Ltd.
Rodolfi L, Zittelli GC, Bassi N, et al: Microalgae for oil: strain selection, induction of lipid synthesis and outdoor mass cultivation in a low-cost photobioreactor, *Biotechnol Bioeng* 102(1):100–112, 2009.
Schirrmeister BE, de Vos JM, Antonelli A, Bagheri HC: Evolution of multicellularity coincided with increased diversification of cyanobacteria and the Great Oxidation Event, *Proc Natl Acad Sci* 110(5):1791–1796, 2013.
Souliés A, Pruvost J, Legrand J, Castelain C, Burghelea TI: Rheological properties of suspensions of the green microalga *Chlorella vulgaris* at various volume fractions, *Rheol Acta* 52(6):589–605, 2013.
Stramski D, Bricaud A, Morel A: Modeling the inherent optical properties of the ocean based on the detailed composition of the planktonic community, *Appl Opt* 40(18):2929–2945, 2001.
Stramski D, Mobley CD: Effects of microbial particles on oceanic optics: a database of single-particle optical properties, *Limnol Oceanogr* 42(3):538–549, 1997.
Stramski D, Morel A, Bricaud A: Modeling the light attenuation and scattering by spherical phytoplanktonic cells: a retrieval of the bulk refractive index, *Appl Opt* 27(19):3954–3956, 1988.
Sukenik A, Levy R, Levy Y, Falkowski P, Dubinsky Z: Optimizing algal biomass production in an outdoor pond: a simulation model, *J Appl Phycol* 0921-89713:191–201, 1991.
Takache H, Christophe G, Cornet JF, Pruvost J: Experimental and theoretical assessment of maximum productivities for the microalgae *Chlamydomonas reinhardtii* in two different geometries of photobioreactors, *Biotechnol Prog* 26(2):431–440, 2010.
Takache H, Pruvost J, Cornet JF: Kinetic modeling of the photosynthetic growth of *Chlamydomonas reinhardtii* in a photobioreactor, *Biotechnol Prog* 28(3):681–692, 2012.
Tiwari A, Pandey A: Cyanobacterial hydrogen production–a step towards clean environment, *Int J Hydrog Energy* 37(1):139–150, 2012.
Traverse A: Paleopalynology, Topics in geobiology (Dordrecht, The Netherlandds, 2007, Springer.
van de Hulst HC: *Light scattering by small particles,* Mineola, NY, 2012, Courier Dover Publications.
Van Vooren G, Grand FL, Legrand J, Cuine S, Peltier G, Pruvost J: Investigation of fatty acids accumulation in *Nannochloropsis oculata* for biodiesel application, *Bioresour Technol* 124:421–432, 2012.
Wait JR: Scattering of a plane wave from a circular dielectric cylinder at oblique incidence, *Can J Phys* 33(5):189–195, 1955.
Waterman PC: Matrix formulation of electromagnetic scattering, *Proc Inst Electr Electron Eng* 53(8):805–812, 1965.

Williams PJleB, Laurens LML: Microalgae as biodiesel and biomass feedstocks: review and analysis of the biochemistry, energetics and economics, *Energy Environ Sci* 3:554–590, 2010.

Wolk CP, Simon RD: Pigments and lipids of heterocysts, *Planta* 86:92–97, 1969.

Xu YL: Electromagnetic scattering by an aggregate of spheres: far field, *Appl Opt* 36(36):9496–9508, 1997.

Yun YS, Park JM: Kinetic modeling of the light-dependent photosynthetic activity of the green microalga *Chlorella vulgaris*, *Biotechnol Bioeng* 83(3):303–311, 2003.